CHEMISTRY DOCTORAL SCHOOL

ANALYTICAL CHEMISTRY, COLLOID-AND ENVIRONMENTAL CHEMISTRY, ELECTROCHEMSTRY

ACCIARO ROBERTA

Ph.D. Thesis

Tuning the internal structure of pNIPAm-based microgel particles and multilayers

Supervisor: Prof. Tibor Gilányi

Co-Supervisor: Dr. Imre Varga

Head of Doctoral School: Prof. Dr. György Inzelt

Program Leader: Prof. Dr. Gyula Záray

Eötvös Loránd Unviversity

Institute of Chemistry, Department of Physical Chemistry

Laboratory of Interfaces and Nanosize Systems

Budapest

2011

CONTENTS

ACKNOWLEDGMENTS

I am grateful to many people who helped me with the preparation of this thesis.

First of all I would like to thank my supervisor Prof. Tibor Gilányi for giving me the chance to become part of his research group and for sharing his professional knowledge and useful advices.

A special thanks to Dr. Imre Varga, who involved me in his scientific projects, and provided high quality teaching, help and support with patience and enthusiasm.

To my dear colleagues, to Dr. Mészáros Róbert and to the laboratory technicians who played an important role in making me feeling 'at home' with their reliable help and sincere friendship.

Last but not least to Péter and my family for their love, support and for always believing in me. Thank you!

INTRODUCTION

Soft materials have gained much attention as candidates in many industrial and medical applications. Among them stimuli-responsive hydrogels have attracted a widespread interest in the past decades. These materials can give reversible non-linear response in their swelling and shrinking to environmental stimuli. The stimuli that have been investigated to induce changes in polymer gels are diverse, and they include temperature, pH, solvent and ionic composition, electric field, light intensity, and introduction of specific molecules. Responsive polymers can also be used for the formation of interfacial layers, which allows e.g. the switching of the interface between hydrophobic and hydrophilic, adhesive and repellent, or able to release or able to adsorb some species.

A major disadvantage of bulk macroscopic hydrogels is their slow response to the changes in the external conditions. However, this problem can be overcome by the preparation of microgels. Microgel particles are cross-linked macromolecules that swell in the solvent. They have several orders of magnitudes smaller characteristic dimensions than that of the macrogels resulting in a considerably accelerated kinetic behavior. Besides their technical applications (e.g. surface coatings, rheological control and stabilizing agents) microgels are promising candidates for the development of biochemical and biomedical applications, controlled drug delivery systems, heavy metal scavengers, etc.

Of great importance is the potential use of stimuli responsive microgels as biomaterials. Many investigations demonstrated that they can be suitable to fabricate drug-releasing systems or they can be employed as tissue engineering matrices. In the literature the promising role of pNIPAm based microgel as nanocontainers is emphasized. The application of the microgels for controlled drug release is in focus, however despite the intense work in the field still several challenges have to be overcome. The goal of my PhD work was to address some of these challenges:

1. Several investigations in the literature report the employment of pNIPAm based microgels to prepare multilayer systems for controlled molecule release at interfaces. In these studies the multilayers are build up by the well known layer-by-layer deposition technique by alternating negatively charged p(NIPA-co-AAc) microgels and a positively charged polyelectrolyte. However, since the applied polyelectrolyte interpenetrates the microgel particles, the microgel swelling is inhibited and as a consequence the microgel loading and release capacity becomes limited. My aim was to form a microgel multilayer, where swelling characteristics of the microgel

particles is not altered by the build-up procedure. To achieve my goal I used an innovative cationic material called microfibrilleted cellulose fiber in place of the classical polyelectrolytes, to hinder the interpenetration of the oppositely charged components and to form an open structure to improve the loading-release characteristics of the microgel multilayers.

2. The capacity of the microgel particles to incorporate and immobilize large biomacromolecules is limited by their mesh size distribution, which is related to the internal structure of the microgel particles. Though, in an optimal case the microgel particle should have a uniform mesh size distribution, in practice it is well known that pNIPAm microgels have a highly inhomogeneous internal structure due to the non uniform cross-link distribution within the particles. The necessity to prepare and use microgel particles with a homogeneous internal structure has been discussed and emphasized by many research groups but it has not been solved yet. My aim was to develop a synthetic method that allowed the preparation of homogenously cross-linked microgel particles.

3. Biocompatibility is a crucial factor for the medical application of the microgels. In their swollen state pNIPAm microgels are “stealth” particles for drug delivery because they are able to evade the body immune system. The large water content in the swollen state makes them biocompatible and optimal biomolecular containers. However, the delivery of charged molecules (e.g. drugs, or proteins) requires the application of oppositely charged microgels, which in turn collapse and loose their biocompatibility as well as their colloid stability when loaded with the target molecule in a maximum amount. My last aim was to prepare charged microgel particles with an uncharged biocompatible outer shell (PEO) to overcome these difficulties. Furthermore, to minimize the costs associated with the preparation of core/shell microgels I developed a method that allowed the formation of the core/shell structure in a single synthetic reaction.

I. LITERATURE REVIEW

I.1. Gels and hydrogels

As a state of matter gels are considered to be semi-solid materials with intermediate characteristics of a solid and a liquid. As a solid, gels maintain the original shape showing elastic behaviour under mild shear stress, as a liquid they allow mass transport of molecules smaller then their pore size. The polymer gels are also described as colloidal polymer-solvent systems formed by a three dimensional network of stable interactions. The term of hydrogel, which will be preferably used in this work, simply indicates a gel that strongly swells in water. The network interactions have a primary role in determining the gel dimensional stability and flexibility. They are distinguished into physical and chemical interactions and consequently gels are also categorized as physical and chemical gels[1,2,3].

Physical gels are polymeric networks held together by "weak" attractive forces as hydrophobic, hydrogen bonding or ionic interactions[4,5] acting between the polymer chains. Some of them can be formed from combination of a polyelectrolyte with a multivalent ion, e.g. calcium alginate or from biospecific recognitions, e.g. avidin and polymeric biotin. Since physical interactions are relatively weak, this group of hydrogels has been widely used to release molecules or macromolecules through network disintegration or dissolution induced by changes in physical conditions. In contrast, chemical gels are chemically cross-linked polymeric network. Due to their stability resulting from monomer polymerization in presence of cross-linking agents[6], they are also defined as „permanent". The network swelling can be modulated by cross-link density[7].

Tanaka (1981), defined a gel as a form of matter intermediate between a solid and a liquid which consists of polymers, or long chain molecules, cross-linked to create a tangled network immersed in a liquid medium. The liquid prevents the polymer network from collapsing into a compact mass, while the network prevents the liquid from flowing away. From a morphological point of view gels are also divided into fishnet, lattice and transient.

Fishnet gels are formed by strong cross-links, which compose the strong domains of the gel and which are separated by flexible strands which provide elasticity. In lattice gels the mechanical distinction between cross-links and strands is obscure, but nonetheless, a space-filling structure exits. Transient is a gel in which the structure is not permanent or due to high concentrations cause the polymers to overlap leading to temporary 'cross-links' due to chain entanglement.

Another important classification is based on the hydrogel responsivity. Non-responsive gels are water-swollen materials that are able to retain their shape and integrity upon exposure to various stimuli. Responsive hydrogels are instead prepared from stimuli responsive polymers, thus they undergo solvation changes in response to various environmental changes.

I.2. Stimuli responsive polymers

The non-linear swelling of smart polymers to external stimulus is what makes them so unique and effective. A significant change in structure and properties can be induced by a very small stimulus. Once that change occurs, there is no further change, meaning a predictable all-or-nothing response occurs, with complete uniformity throughout the polymer.

The volume phase transition of responsive hydrogels/gels is a phenomenon that strictly depends on changes in solvation of the polymer (Fig.1). Hydrogels prepared from thermoresponsive polymers, e.g. poly(*N*-isopropylacrylamide) show a transition from a highly swollen to a collapsed state at temperature close to the polymer critical solution temperature. The same effect can be observed for hydrogels prepared from ionisable linear polymers containing weak acidic or basic groups when the environmental pH is varied. In all cases the response of such hydrogels to the external stimulus (temperature or pH change) is non-linear and reversible.

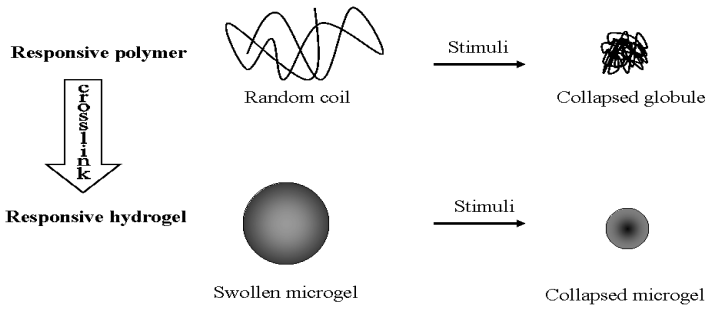

Fig.1 Hydrogels prepared from responsive polymers respond to external stimuli with a volume phase transition.

The thermodynamic description of gel swelling is a classical subject. Flory's theory of gel swelling[8] describes the free energy change of the system accompanying the gel swelling. In

the case of polyelectrolyte gels the total free energy change (ΔF_{tot}) is given as the sum of three independent contributions:

$$\Delta F_{tot} = \Delta F_{el} + \Delta F_{mix} + \Delta F_{ion} \tag{1}$$

where (ΔF_{el}) denotes the free energy of elastic deformation of the gel network, (ΔF_{mix}) is the free energy of the mixing of the polymer chains and the solvent molecules within the swollen hydrogel, and (ΔF_{ion}) is related to the concentration difference of the mobile ions between the inside and the outside of the gel. Traditionally the gel swelling is described in terms of the osmotic pressure ($\Delta\pi_{tot}$), which can be derived from the free energy change of the system:

$$\Delta\pi_{tot} = -V_1 \partial\Delta F_{tot} / \partial n_1 = \Delta\pi_{el} + \Delta\pi_{mix} + \Delta\pi_{ion} \tag{2}$$

where $\Delta\pi_{el}$, $\Delta\pi_{mix}$, $\Delta\pi_{ion}$ are the elastic, mixing and ionic contributions to the total osmotic pressure, respectively, V_1 is the molar volume of the solvent and n_1 amount of solvent in moles.

The elastic contribution of the osmotic pressure can be given by the theory of rubber elasticity if the gel is formed by flexible polymer chains.

$$\Delta\pi_{el} = -ART\nu\Phi^{1/3}, \tag{3}$$

where ν is the concentration of the polymer chains, Φ is the volume fraction of the polymer within the gel, R is the gas constant and T is the absolute temperature. However, in the case of polyelectrolytes the polymer chains are highly extended, thus it has been shown that the elastic pressure for polyelectrolyte gels can be described more realistically by theories based on non-Gaussian chain statistics[9]. The osmotic pressure term related to the mixing of the polymer chains and the solvent can be described by the Flory-Huggins equation

$$\Delta\pi_{mix} = -\frac{RT}{V_1}\left[ln(1-\Phi) + (1-P^{-1})\Phi + \chi\Phi^2\right] \tag{4}$$

where P is the degree of polymerization ($P = \infty$ for cross-linked gels) and χ is the Flory-Huggins interaction parameter.

The concentration difference of the mobile ions between the gel and its equilibrium solution is the consequence of the requirement that macroscopic charge separation cannot take place, i.e. the counterions of the polyelectrolyte segments must stay within the gel. This concentration difference results in an osmotic pressure between the gel and its equilibrium solution, which can be given by the Donnan theory:

$$\Delta\pi_{ion} = RT\sum_{j=1}^{N}\left(c_j^{gel} - c_j^{sol}\right) \quad (5)$$

where c_j^{gel} *and* c_j^{sol} denote the concentrations of a small ion type *j* within the gel and in the equilibrium solution, respectively, and *N* is the number of different types of mobile ions in the system.

In the case of responsive polymer gels the external stimuli dependent swelling is usually the consequence of the tuning of the osmotic pressure term

Until the end of 1970s, only polymer gels showing linear change in their swelling were known. In 1978 Tanaka discovered that partially hydrolysed poly(acrylamide) gels show an abrupt gel collapse as a function of temperature or solvent composition[10]. It has been shown that while the gel collapse is related to the change of the solvent quality due to e.g. temperature changes, the abruptness of the change in the gel swelling is related to the large osmotic pressure caused by the counterions of the charged segments. Since the pioneering discovery of Tanaka several other responsive polymers have been prepared and response to stimuli like e.g. light or presence of specific molecules has been developed.

Bawa et al. categorized some of the responsive polymers depending on the stimuli sensitivity[11].

Thermoresponsive polymers

Temperature-sensitive hydrogels are probably the most commonly studied responsive polymers in drug delivery research. Many polymers exhibit a temperature-responsive phase transition property. They are characterized to carry either moderately hydrophobic moieties e.g. methyl, ethyl, propyl groups and hydrophilic segments. The equilibrium between hydrophilic and hydrophobic interactions is thermally regulated and determines the solvation state of the polymer. Of great importance are those polymers characterized to posses a lower critical solution temperature (LCST) around the body temperature. Under the LCST, hydrophilic interactions, e.g. hydrogen bonding, are predominating and the polymer chains are solvated. Increasing the temperature above the LCST, the hydrophobic interactions among polymer chains prevail and phase separation occurs[12,13] The solubility decreases with increasing temperature. A typical example of thermoresponsive polymers showing LCST is the poly(*N*-isopropylacrilamide)[14], its temperature dependent structural conformation transition is showed in Fig.2.

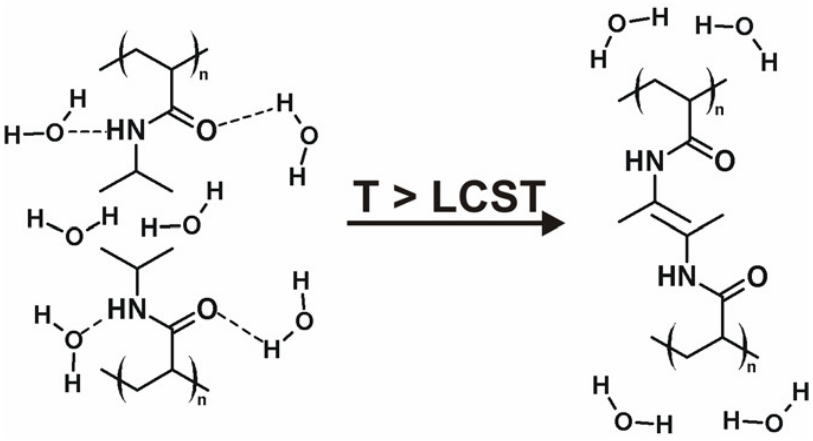

Fig.2 Molecular level view of the pNIPAm structure. At temperatures below the LCST water is a good solvent for pNIPAm but as the temperature of the solution is increased the polymer becomes a better solvent for itself resulting in an entropy-driven expulsion of water.

The LCST can be changed by adjusting the ratio of hydrophilic and hydrophobic segments in the polymer. In general as the polymer chain contains more hydrophobic constituents LCST becomes lower[15]. One way is to make copolymers of hydrophobic (NIPAM) and hydrophilic (Acrylic acid) monomers[16].

Another class of thermoresponsive polymers, e.g. poly(*N*,*N*-dimethylacrylamide), shows an upper critical solution temperature (UCST)[17] For this group solubility decreases by temperature decrease. Other polymers, such as poly(o-chlorostyrene), show both an upper and a lower critical solution temperature[18] as depicted in Fig.3 .

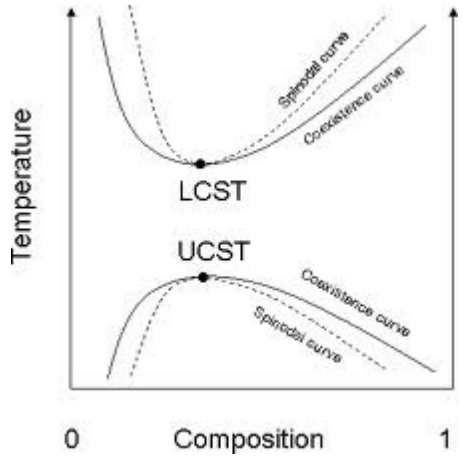

Fig. 3 A typical polymer solution phase behaviour including two critical points: LCST and UCST.

pH-responsive polymers or polyelectolytes

Changes in environmental pH lead to solvation changes of these responsive polymers due to the presence of weakly ionisable pending groups[19,10] Columbic repulsions predominate over hydrophobic attraction of polymer chains if moieties are ionized. The most commonly investigated pH responsive polymers are the poly(acrylic acid), poly(meth acrylic acid), poly(diethylaminoethyl methacrylate). Poly(acrylic acid) is generally used as co-monomer to confer pNIPA pH responsivity through integration of carboxylic groups. The copolymer is known as poly(*N*-isopropylacrylamide-*co*-acrylicacid), p(NIPA-*co*-AAc)[20,21].

pH responsive polymers can be distinguished into two groups: acidic groups bearing e.g. –COOH, which swell at basic pH, and basic groups bearing e.g. –NH2, which swell in acidic environment. Poly(acrylic acid) is an example of the former class and chitosan an example of the latter.

This group of polymers can also be classified as "ionic-strength responsive", since the salt concentration reduces the repulsive electrostatic interactions between the polymeric chains, which results in dominating hydrophobic attraction.

The phase transition of the gels occurs in a small range close by the apparent acid dissociation constant pK_a of the hydrogel, which is mostly identical with the pK_a of the ionisable group. Approximately, at the apparent pK_a of the gel the ionisation begins and it is accompanied by a drastic swelling of the hydrogel. If the ionisation of the ionisable component is completed the swelling process stops. Further pH increase only increases the ionic strength resulting in the decrease of the osmotic pressure and leading to the shrinking of the gel. Figure 4 shows the effect of pH on the swelling of different types of polyelectrolyte gels.

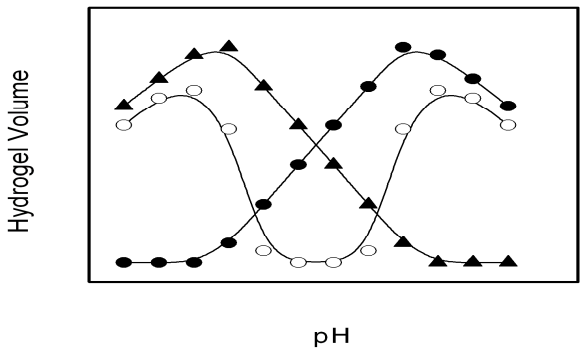

Fig. 4 Phase transition behaviour of polyelectrolyte hydrogels**.** Acidic hydrogels (●) are ionised by deprotonation in basic solutions. Basic hydrogels (▲) swell in acidic solutions due to the ionisation of their basic groups by protonation. Amphiphilic hydrogels (o) contain both acidic and basic groups, therefore they show two phase transitions.

Other types of responsive polymers

In addition to temperature and pH responsive polymers several other types of responsive polymers have been developed. Electro-responsive polymers are basically polyelectrolytes[22,23]. In the presence of an external electric field they deform due to anisotropic swelling and deswelling as charged ions are directed towards the anode or cathode side of the gel. E.g. hydrogels made of poly(2-acrylamido-2-methylpropane sulfonic acid–co-*n*-butylmethacrylate) were able to release edrophonium chloride and hydrocortisone in a pulsatile manner using electric current[24].

Light responsive polymers are prepared by introduction of a light sensitive molecule into the polymer network. E.g. UV-light sensitive hydrogel was synthesized by introducing a leuco derivative molecule, (bis-4-di-methylamino)phenylmethyl leucocyanide into the gel network. The leuco derivatives are normally neutral molecules but dissociate into ion pairs under ultraviolet irradiation. The presence of such ionic species produces an increase in osmotic pressure and induces the gel to swell[25].

Ultrasonically responsive polymers are generally bierodible ones. When exposed to ultrasound these polymers heat up and degrade. Some of them were evaluated as drug carrier matrices e.g. polyglycolide, polylactide, bis(p-carboxyphen-oxy)alkane anhydride to release molecules such as *p*-nitroaniline, *p*-amino-hippurate, bovine serum albumin and insulin. It is believed that the ultrasound causes a local increase in temperature in the delivery system, which facilitates the molecules diffusion[26].

Research of stimuli-responsive polymers is steadily gaining momentum and more novel polymers are being synthesized to be incorporated into innovative delivery systems intended for site-specific and self-regulated drug delivery. Stimuli-responsive polymers are also immensely valuable in applications such as bioseparation of proteins and other bio-particles for basic life science research as well as industrial applications.

I.3. Microgels

According to their size hydrogels are differentiated in macro- and microgels. The microgel range varies from the nanometer to the micrometer scale (10nm-1μm), while the macrogels have several orders of magnitudes larger dimensions. The size of the hydrogels is a crucial factor that determines their properties. Because of its small size, stimuli responsive microgels respond to environmental changes much faster than macrogel does. It has been demonstrated that the deswelling can take hours or even days for macrogels. The kinetic of gel swelling was described by Tanaka and Fillmore [27].

$$\tau \approx R^2/D \tag{6}$$

where τ is the time of gel swelling or collapse, R the gel size and D the cooperative diffusion coefficient of the solvent, which describes the motion of a number of molecules in a density gradient. For typical polymer gels, D is on the order of 10^{-7}-10^{-6} cm^2/s, depending on the polymer concentration, cross-link density, etc. However, it is not easy to increase the value of D by a factor of 10^2 or more. Therefore, a reduction of gel size has been thought to be the only way to achieve quick response as shown in Figure5.

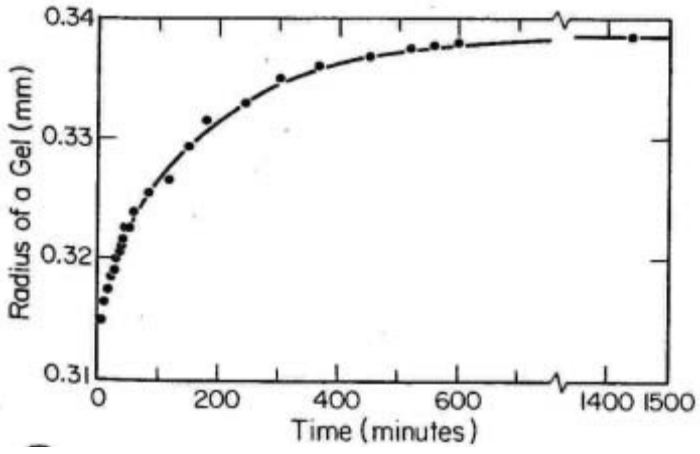

Fig. 5 Time of gel swelling in gels of different radius.

The characteristic properties mentioned above make microgels attractive in many applications and some of them are mentioned below.

(I) Drug delivery systems: Microgels show high biocompatibility in the swollen state due to their high water content. Moreover they are suitable for controlled release when prepared as responsive particles[28]. Comparing to the normal particulate drug carrier dispersions they offer higher colloidal stability, ease of preparation, particle size control and controlled functionalization[29].

(II) Sensor transducers / Biomimetic actuators: Stimuli-responsive microgels can convert the non-electrical changes of properties into an electrical signal or mechanical work[30]. Transducers can exploit the mechanical work performed by hydrogels or observe alteration in hydrogel properties such as density, volume and stiffness[31].

(III) Thermoresponsive surfaces. Grafting thermoresponsive microgels onto the surfaces endows the surface with considerable thermoresponsive properties, e.g the surface is of hydrophilic character below the critical temperature of the polymer transition and hydrophobic above it[32].

Poly(*N*-isopropylacrylamide) (pNIPAm) is certainly the most studied polymer employed in forming responsive microgels. pNIPAm belongs to the class of thermo-responsive polymers. It undergoes a coil-to-globule transition in aqueous media at ~32°C, *i.e.* at its "lower critical solution temperature" (LCST). When the polymer chains are cross-linked in a network forming a microgel, the responsivity manifests itself as a volume collapse arising from the expulsion of the solvent (water). This transition temperature is referred to as a "volume phase transition temperature" (VPTT), which is generally slightly higher than the LCST of the corresponding linear polymer[33].

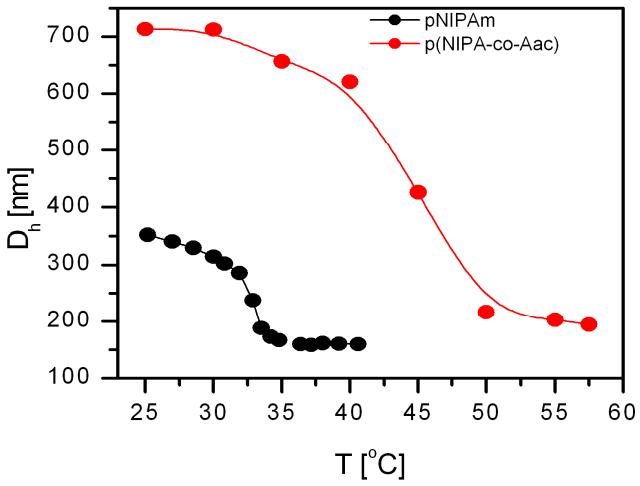

Fig.6 The change of the hydrodynamic size of the pNIPAm and p(NIPA-co-AAc) particles (pH≈4.5) hydrogels with the temperature

The volume phase transition of the microgels can also be tuned by copolymerization with hydrophilic comonomers. NIPAm has been copolymerized with a wide range of co-monomers, e.g. with acrylic acid[21], methacrylic acid[34], maleic acid[35],vinylacetic acid[36,37] and allyl-acetic acid[38]. Poly(N-isopropylacrilamide-co-acrylicacid) (pNIPA-co-AAc) is one of the most intensively investigated pNIPAM copolymers and has the character of a polyelectrolyte gel. Addition of acrylic acid to the microgel network leads to modulation of the VPTT that is shifted to higher value (Fig.6) if the pH is higher than the pK_a of the acrylic acid.

The swelling of the pNIPAm based microgels is also modulated by the cross-linker content. McPhee et al. prepared a series of particles with varying bisacrilamide (BA) content demonstrating that the lower BA concentration leads to the formation of larger particles[39].

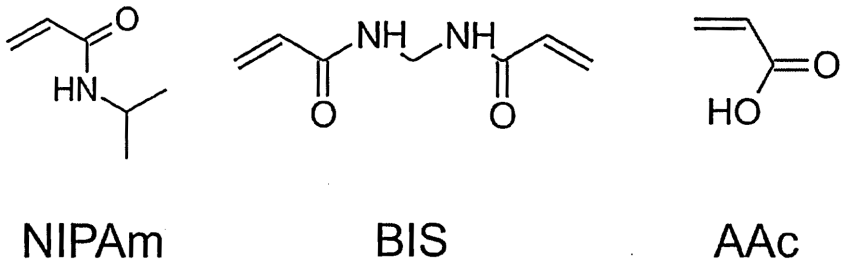

Fig.7 NIPAm, BIS and AAc monomers, employed in the preparation of p(NIPAm-co-Aac) microgel particles

Highly cross-linked pNIPAm based microgel aqueous solution appears turbid and milk-like to the eye. The reason is behind the fact that the cross-linker is heterogeneously distributed into the microgel particles having a higher refractive index than the surrounding water.

Above the LCST of the pNIPAm based microgel the particles deswell expelling most of the water and the turbidity is even more pronounced. Solutions of low cross-linked density pNIPAm microgels and charge bearing pNIPAm microgel particles on the contrary incorporate more water resulting in a lower turbidity.

Microgel particles are also of great interest due to their inherent colloidal stability both in the swollen and in the collapsed state. In fact charged fragments arising from the initiator are present on the particle surface generating an electrostatic stabilization independently of the degree of swelling. Furthermore in the swollen state the presence of polymer dangling chains on the particle surface increases the particle stabilization by a steric contribution. Van der Waals attraction can also be neglected since the Hamaker constant (solvent-polymer interaction parameter) approaches to zero. In the collapsed state, therefore under poor solvency conditions, although the steric stabilization becomes less effective and the van der Waals attraction is most pronounced, the electrostatic repulsion is still effective to ensure particle stability. Different is the case of electrically charged polyelectrolytes as e.g. p(NIPAm-co-AAc), at low pH values and at temperature values over the VPTt where the $-COO^-$ protonation and the initiator charges burial lead to particles aggregation and precipitation.

I.3.1. Microgel synthesis

The most commonly used method to prepare pNIPAm microgels (called surfactant-free emulsion polymerization (SFEP) or surfactant free precipitation polymerization (SFPP)) was reported first by Pelton and Chibante[40]. Monomers and cross-linker (generally BA) are dissolved in water. Oxygen is removed by N_2 purging. The temperature is raised above the LCST (typically to 60-80°C), then the reaction is initiated by the addition of amonium persulfate (APS). By radical propagation the polymer chains grow, then at a critical length collapse forming precursor particles, which aggregate to each other resulting in larger particles (Fig. 8). Due to the accumulation of the initiator charges at the interface of the aggregated particles they become stable. Further polymerization takes place within these particles giving rise to the final cross-linked microgels. A variant of the described method was proposed by McPhee[39] to control the particles size. It was demonstrated that introducing sodium dodecyl sulphate (SDS) to the monomer solution the particles diameter can be controlled due to the adsorption of SDS on the aggregates of the precursor particles that facilitate their stabilization. With increasing SDS concentration the size of the resulting microgel particles becomes smaller. It should be emphasized that SFEP and SFPP gives rise to highly monodispersed pNIPAm microgels.

Fig. 8 Microgel particles formation by homogeneous nucleation

An alternative technique to prepare stimuli responsive hydrogels is the so-called inverse emulsion polymerization. An aqueous solution of the hydrophilic monomer is dispersed in a continuous liophilic medium using surfactants, which promote the formation of water-in-oil (W/O) emulsion. The technique is applicable to a wide variety of hydrophilic monomers and oil media and results in samples with average particle sizes smaller then 0.05 μm[41].

I.3.2. Core-shell microgels

Core-shell microgels can be divided into two groups: 1) the core is a non-hydrogel material and the shell is a hydrogel and 2) core and shell are both hydrogels. Belonging to the first group it is worth mentioning the preparation by Dingenouts et al.[42] of particles formed by a polystyrene-co-pNIPAm core and cross-linked pNIPAm shell as well as the polystyrene core and "hairy" pNIPAm shell fabricated by Xiao et al.[43]. Based on the same approach Zha et al.[44] used silica particles functionalized with vinyl groups as core material and attached by PP a pNIPAm shell. The silica core was then dissolved by HF, which led to the formation of hollow pNIPAm capsules. The second group of core-shell particles, consisting of hydrogel-like core and shell was first prepared by Lyon *et al.*, who applied a two stage precipitation polymerization[45]. First a microgel was prepared with standard precipitation polymerization, then after extensive cleaning the prepared microgels were used as seeds in a second precipitation polymerization step to form the outer shell of the particles. No increase in polydispersity was observed as all the oligomers formed in solution precipitate onto the preformed core particles. Berndt and Richtering[46] have also synthesized core-shell particles consisting of a pNIPAm core and a p(N-isopropylmethylacrylamide) shell. Investigations on particle thermoresponsivity showed two phase transition behaviour due to the different VPTT of the two constituting polymers.

I.3.3. Microgel structure

A considerable effort have been made in the literature to shed light on the internal structure of hydrogels since the morphology of the microgel particles has a strong influence on many properties such as the swelling and the mass transport through the polymeric network. Many techniques were used for this purpose with the common result that PP and SFPP preparation methods produce highly inhomogeneous microgel particles. Wu and Pelton were the first who reported that during the polymerization process the cross-linker was faster incorporated into the gel then NIPAm monomers leading to the formation of heterogeneous inner microgel structure[47]. Light scattering is one of the most widely used method for structural analysis[48,49]. A combination of the static and dynamic light scattering measurements by Varga et al.[7] suggested that the microgel particles have an inhomogeneous internal structure that depends on the degree of cross-linking. The most highly cross-linked microgels retain a particle character and exhibit a Gaussian segment density distribution in their swollen state. However, with decreasing cross-link density the microgel particles can be better described

as core/shell structures formed by a highly cross-linked core and a shell of dangling polymer chains.

Crowther *et al*. used SANS for the characterization of the microstructure of pNIPAm microgels as a function of temperature[50.] They observed Porod scattering in the collapsed state of the microgel particles and a combination of Porod and Ornstein-Zernike scattering below the phase transition temperature. These results indicate that microgels form compact particles with sharp phase boundary in their collapsed state but a significant fraction of the polymer chains occupy a solution-like microenvironment below the VPTT. Kratz et al. investigated the effect of crosslink density[51] and the effect of the chemical nature of the cross-linker monomer[52] on the microstructure of microgels and they observed similar structural features. Later, Fernandez-Barbero et al.[53] as well as Sounders et al.[54] interpreted the SANS results in terms of the formation of a cross-linker rich core and a low segment density shell at the surface of the particles. These results were formally summarized in a core-shell form factor by Stieger et al.[55] describing a uniform chain density in the microgel core and gradual decay in the segment density toward the surface of the microgel.

Two possible particle structures have been proposed in the literature[56], which are depicted in Fig. 9. Both structures take into account the aggregation and growth during polymerization and they show a core-shell organization where the inner part has a higher cross-link density then the outer region. Core and shell in (a) consist of aggregated nanoparticles while in (b) they have uniform structure and mesh size.

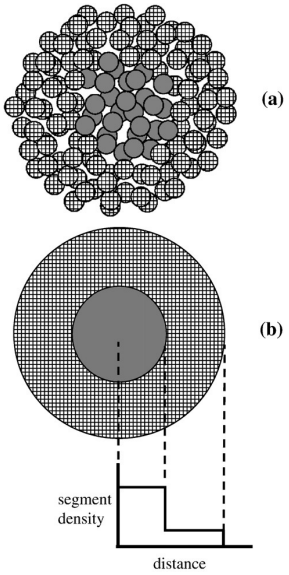

Fig.9 Two possible morphology for the microgel particles as presented by Saunders.

Though, the two structures are indistinguishable by scattering techniques, high resolution SEM images of poly(NIPAM/BA) microgel particles presented by Saunders (Fig. 10) reveals a nodular morphology. This is generally consistent with the aggregation of nanoparticles depicted for structure (a) in Fig. 9.

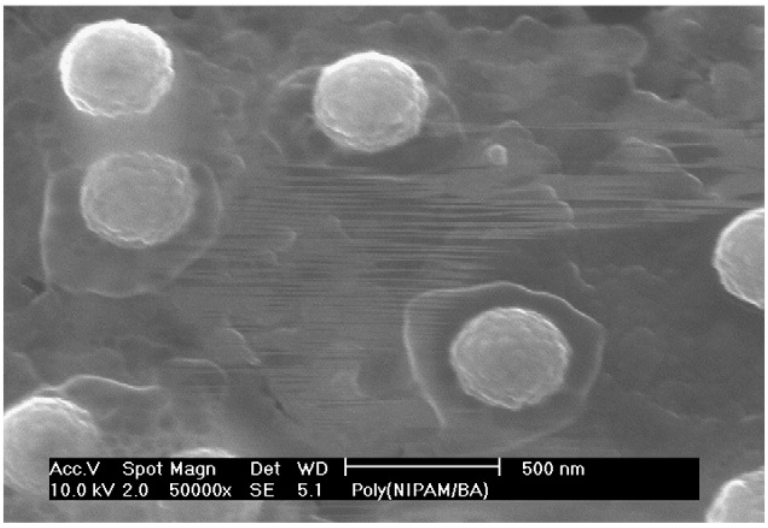

Fig.10 SEM of poly(NIPAM/BA) microgel particles.

To describe that different monomers are incorporated into the microgel particles with different rates, Hoare[57] et al. developed a model to predict the particle microstructure and local compositional gradients within the microgel particles. The model is based on the assumption that the homogeneous nucleation is followed by the inside out growth of the particles. In this model the monomer consumption rates are calculated from the reactivity ratios between each pair of monomers used in the microgel preparation, which were derived from the initial propagation rates for the homopolymerization of each of the monomers, and the composition of the initial monomer mixture, all of which are experimentally measurable parameters. The approach permitted to predict carboxylic functional group distribution (radial density) of pNIPAm based microgels copolymerized with different comonomers. The distribution was also measured experimentally via transmition electron microscopy after the carboxylic groups were selectively stained by uranyl acetate. The calculated and the experimental morphologies observed by TEM were correlated confirming the hypothesis of the inside-out growth of the particles. Furthermore, using local swelling calculations it was demonstrated that microgel particles that contained the same amount of cross-linker and functional monomer, but which had different radial functional monomer distribution exhibited more than a five-fold difference in the magnitude of their pH induced swelling.

The results clearly highlight the impact of particle heterogeneity on particles properties and the necessity to develop a method that allows the preparation of microgel particles with uniform crosslink distribution.

I.4. Polymer-surfactant interaction

Polymers and surfactants are present together in many formulations, for example in foods, surface coatings, pharmaceuticals and cosmetics. Therefore, understanding the interaction of polymers and surfactant is important from both a theoretical and an industrial point of view. Informations about these interactions are provided by the surfactant binding isotherm (the amount of surfactant bound to unit mass of polymer, B) which can be obtained as follows:

$$B = (c_o - c_{free})/c_{pol} \tag{7}$$

where c_{pol} is the polymer concentration and c_o and c_{free} are the analytical (total) and the equilibrium monomer surfactant concentrations, respectively.

Determination of the monomer surfactant concentration (c_{free}) can be based either on indirect or direct activity measurements. In a typical indirect experimental setup equilibrium is established between the polymer-surfactant system (Cell P/S) and a polymer free surfactant solution (Reference system, Cell Ref.). In the case of ionic surfactant the thermodynamic condition of equilibrium is the constancy of the mean chemical potential of the surfactant, which reduces to the equality of the mean surfactant activity in the two cells ($a_{\pm,P/S} = a_{\pm,ref}$). A convenient direct activity measurement can be conduct by directly measuring the surfactant activity by means of surfactant selective electrodes. As a general assumption the measured mean surfactant activity is practically equal to the monomer surfactant concentration. However, Gilányi et al.[58] showed that this assumption is not valid in the presence of macroions (e.g. polyelectrolytes, surfactant aggregates), which can affect the spatial distribution of the small ions (e.g. surfactants) in the system. Therefore, taking into account the electrostatic interactions of the macroions and the surfactant ions the following expression was derived:

$$c_{free} = c_{\pm,\,Surf}\langle e^{y}\rangle \tag{8}$$

where $y = e\Psi/kT$ is the reduced electrical potential with a reference potential $\Psi = 0$ in the polymer free reference system and $\langle\ \rangle$ denotes volume averaging. Using the above expression the binding isotherm can be calculated as:

$$B_{pol} = c_0 - c_{\pm,\,Surf}\langle e^{y}\rangle / c_{pol} \tag{9}$$

One possible way to calculate $\langle e^y \rangle$ is to measure the activity of a probe electrolyte added to the system in trace amounts; as an alternative it is possible to determine the surfactant activity in the presence of a large amount of inert electrolyte, when $\langle e^y \rangle$ becomes practically equal to one.

Surfactant binding can either be a cooperative or non-cooperative process. In the case of cooperative binding the surfactant molecules bind in the form of micelle-like surfactant aggregates along the polymer chain. In this case the binding starts above a finite surfactant concentration called the critical aggregation concentration (*cac*). In the case of non-cooperative binding the isotherm is known as Langmuir isotherm and it shows that the surfactant interaction, which occurs in the form of monomer binding, takes place in the presence of any low surfactant concentration. In both cases the binding reaches a plateau value when no more surfactant can bind to the polymer. Finally, the critical micelle concentration (cmc) is reached in the system, when free micelles start forming in the system. A schematic binding isotherm is depicted for both types of binding process in Fig. 11.

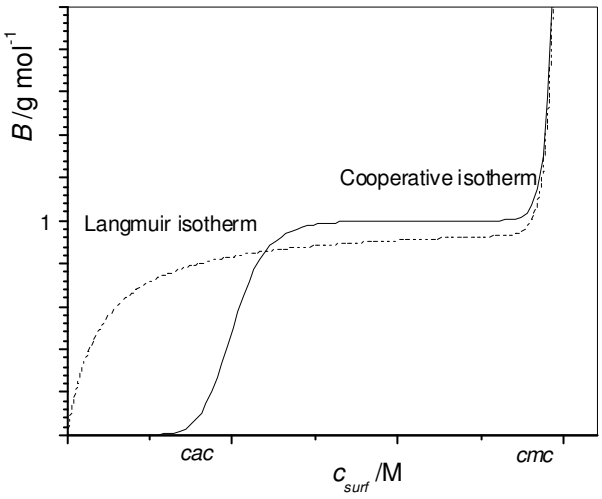

Fig. 11 Binding isotherm.

The experimentally determined binding isotherms give an opportunity for the determination of the cooperativity of the surfactant binding. When the binding isotherm is plotted on a lg-lg scale the slope of the initial part of the binding isotherm is equal to the surfactant aggregation number (*m*):

$$\lg(B) = m \lg(c_{free}) + \text{const} \qquad (10)$$

In the case of oppositely charged polyelectrolyte / surfactant systems, due to the strong electrostatic interaction of the oppositely charged components the interaction is rather strong, giving rise to much smaller cac values than in the case of neutral polymers and ionic surfactants. The most important characteristics of the oppositely charged polyelectrolyte / surfactant systems are demonstrated on the interaction of the hyperbranched polyethylenimine, PEI and oppositely charged sodium dodecyl sulfate SDS[59]. At low surfactant binding a thermodynamically stable solution of the solvated PEI-SDS complexes is formed. With increasing surfactant binding, the net charge of the polyelectrolyte decreases that gives rise to the shrinking of the polymer coil (Fig. 12). As charge neutralization is approached with increasing surfactant binding, the complexes become increasingly compact resulting in increased attractive interaction. At the same time the surface charge density of the complexes decreases giving rise to diminishing electrostatic repulsion. As a consequence in the range of charge neutralization the complexes loose their colloid stability, aggregation and phase separation occurs. If the surfactant concentration is further increased the surfactant ions can adsorb on surface of the PEI-SDS particles leading to the formation of a kinetically stable colloid dispersion.

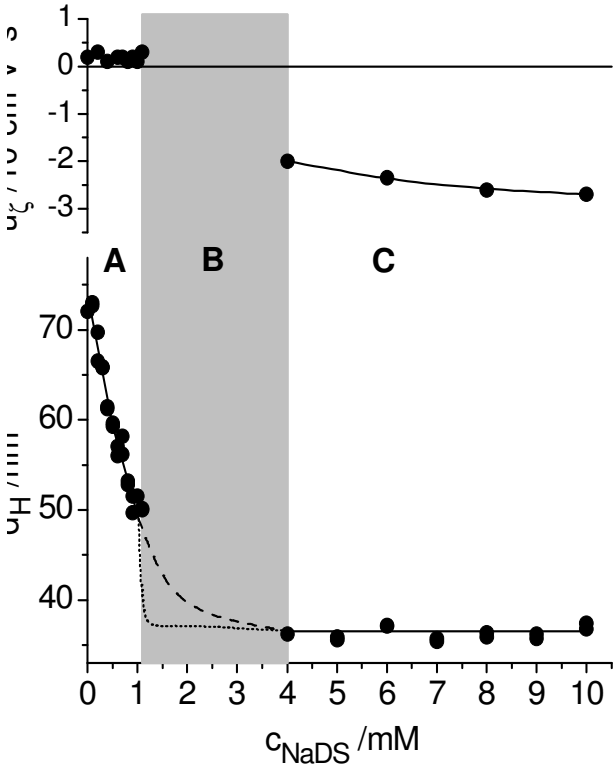

Fig. 12 Electrophoretic mobility and hydrodynamic diameter of PEI as a function of SDS concentration

It has been demonstrated that pNIPAm microgels also interact with ionic surfactants, which have a profound effect on the microgel properties. The interaction of SDS with uncharged

pNIPAm microgels is cooperative and strongly increases the hydrodynamic size of the hydrogel particles due to the formation of SDS aggregates within the microgel network that causes an internal electrostatic repulsion and hence the expansion of the polymer network. It was also shown that the binding occurs as a two step process in the case of highly cross-linked microgel particles: at the first critical surfactant concentration (cac_1) the binding takes place in the slightly cross-linked outer shell of the microgels, while at the cac_2 the surfactant interacts within the highly cross-linked particle core.

I.5. Polyelectrolyte multilayer thin films

The fabrication of responsive nanolayers on solid supports has been of interest for many years for uses in a multitude of applications such as photonic materials[60,61,62] drug delivery systems[63,64,65], sensors[66,67] and chemical resistant surfaces[68,69]. The properties of the multilayer thin films can be tuned by controlling the characteristics of the top surface layer. Responsive surface layers are capable of changing their properties in a reversible manner depending on the conditions exhibited by their environment. These films typically composed of multiple components arranged in a spatially defined fashion. The general approach for the preparation is the well known layer-by-layer deposition (LbL) discovered in 1990's by Decher and co-workers[70]. The process involves a passive adsorption of macromolecules on the surface that has to be previously conditioned to render it charged. The charged surface is then exposed to an oppositely charged polyelectrolyte aqueous solution and the polyelectrolyte is allowed to adsorb to the surface, which gives rise to a charge reversal. After the substrate is rinsed with water it is exposed to an aqueous solution of an oppositely charged polyelectrolyte, which also adsorbs on the surface giving rise to charge reversal (fig.13). The process can be repeated many times to achieve a film with the desired properties and layer number. The technique has many advantages over other thin film fabrication methods including: a self regulated adsorption, possibility to use substrates of any shape, morphology or composition and the control over the order and composition of the individual layers in the films.

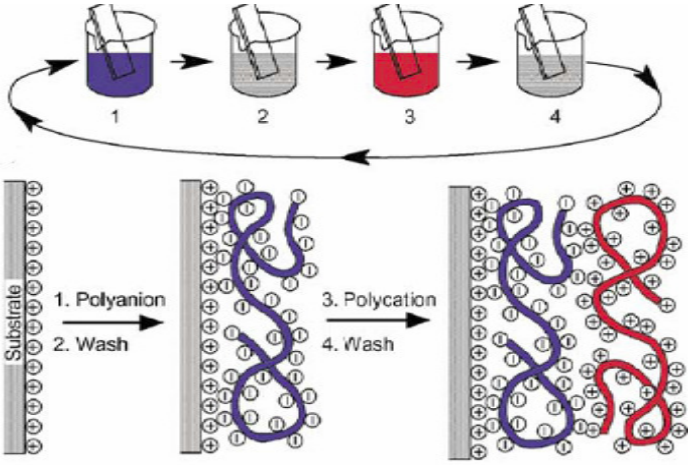

Fig. 13 Layer by layer deposition procedure by dip-coating

An interesting alternative of dip-coating to prepare polyelectrolyte multilayer films is the so called spin-coating. The technique allows for the adsorption of polyelectrolytes to surfaces, in a LbL fashion, taking advantage of a standard spin coater. The advantage over dip-coating is a drastic decrease in deposition time, which is due to the fact that passive adsorption relies on diffusion of polyelectrolytes to surface while this technique enforces interaction of the polyelectrolyte with the surface due to mechanical forces operative during spin-coating.

To utilize pNIPAm microgel particles in the formation of responsive surface layers, several research groups have deposited pNIPAm on solid supports by means of LbL deposition. Vincent and co-workers[71] deposited a pNIPAm microgel monolayer on poly(ethylenimine) activated silica at 50°C. They observed the formation of close-packed monolayers and investigated the effect of the temperature, pH and ionic strength on the stability of the microgel coatings. No desorption of the microgel was detected, but the swelling/deswelling transition of the surface bound microgel particles could be clearly observed. Von Klitzing[72] and co-workers also used dip-coating to deposit microgel monolayers on substrates. They investigated the effect of the substrate pre-coating and pH and they found that the deposition pH has the most important influence on the adsorption density.

Lyon and co-workers used 3-amino-propyltrimethoxysilane (APTMS) functionalized glass surfaces[73,74,75] and cationic alkanethiol functionalized gold surfaces[76] for microgel deposition. They used both dip coating[73] and spin-coating[74,75,77] to build up multilayers of pNIPAm-co-Aac microgels and poly(allylaminehydrochloride) (PAH). To probe the swelling characteristics of the microgel multilayer quartz crystal microbalance (QCM) and surface plasmon resonance (SPR) measurements were used[77]. These measurements revealed that the multilayer structure has different swelling characteristics when it is terminated by a

microgel layer and when it is terminated by a PAH layer. In the latter case the multilayer structure behaved as a homogenous film showing deswelling at high pH (6.5) and swelling in a low pH (3) buffer at room temperature. However, when the microgel was terminated by a pNIPAm layer, this top microgel layer got swollen at high pH, while the layers underneath showed deswelling similarly to the PAH terminated case. These results imply that the interactions of the interdigitated microgel particles and cationic polyelectrolyte (PAH) have a profound effect on the microgel swelling characteristics. Lyon and co-workers have also investigated the loading and release characteristics of the microgel multilayers. They found that when the multilayer was built up by microgel particles preloaded with insulin[76], then the release of the insulin was almost completely suppressed at room temperature. However, when the temperature was increased to 40°C and the microgels were collapsed, a burst of insulin release could be observed. Further studies revealed that the multilayers formed by the insulin preloaded microgels had the capacity to release insulin during many temperature cycles and the magnitude of the release could be controlled by the number of microgel layers. Using doxorubicin as a model drug, Lyon and co-workers have investigated the loading capacity of the microgel multilayers[77]. The drug was loaded into the multilayer by the repeated collapse and swelling of the microgels then the release of the drug was investigated both at room temperature and by temperature cycling. The drug release was also found to be hindered at room temperature but bursts of release could be achieved by temperature cycling. It should also be noted that the drug loading capacity was found to be approximately identical for 10, 20 and 30 layer microgel films. These results imply that due to the interdigitation of the oppositely charged microgel and polyelectrolyte ''glue'' (pdadmac) the microgel particles in the bottom part of the multilayer structure are in a partially collapsed state. Such a partial collapse has also been observed for individual microgel particles when they were coated by oppositely charged polyelectrolytes[78]. Altogether, only a few of the microgel layers on the top of the multilayer structure can be effectively loaded by the drug, which imposes a serious constrain on the loading capacity and on the practical application of the microgel multilayers.

The build-up of a multilayer using other charged colloids is very rare[79]. Self-organized films from cellulose nanofibrils using the LbL-technique has been reported by Wagberg et al.[80] and by Aulin et al.[81,82]. The latter investigation demonstrated that it is possible to form multilayers using only charge-stabilized colloid MFC. MFC refers to cellulose I nanofibrils disintegrated from plant cell walls. The fibrils are 5–10 nm thick and have a length of up to 1 μm and can, as such, be regarded as nanofibers. Due to their high crystallinity[83], aspect

ratio and stiffness, the potential utilization in advanced applications as a renewable, abundant and biodegradable natural product has already attracted an increasing interest[84]. For example, MFC has a large potential for applications in high-strength biocomposites. The preparation of MFC derived from wood was introduced by Turbak et al.[85] and Herrick et al.[86] more than two decades ago. Through a homogenization process, wood fibers are disintegrated, to give a material where the fibers are degraded and where their sub-structural fibrils are liberated from the mesostructure of the fibre wall (fig.14).

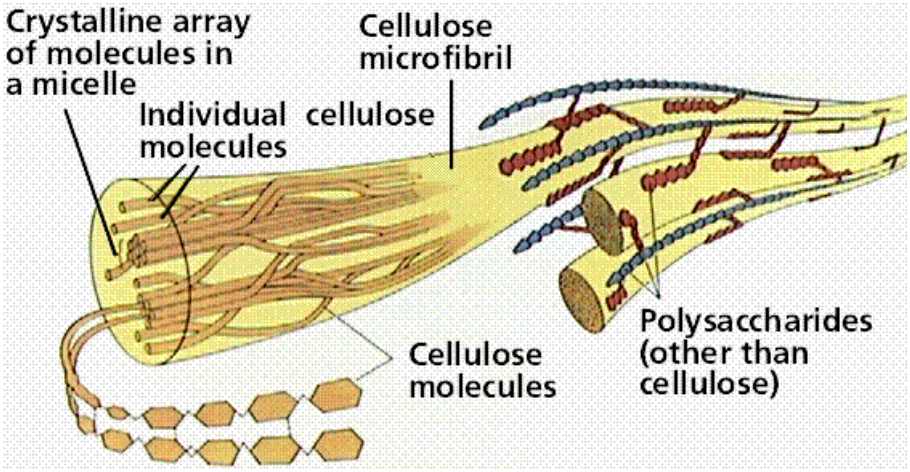

Fig. 14 Arrangement of fibrils, microfibrils and cellulose in cell walls.

II. EXPERIMENTAL

II.1. Materials

All reagents including the *N*-Isopropylacrylamide monomer (NIPAm), the *N*,*N*′-methylenebis(acrylamide) cross-linker (BIS) and the ammonium persulfate initiator (APS) for the microgel synthesis, branched polyethylenimine (PEI M_w = 750 000), fluorescein isothiocyanate isomer I (FITC), poly-(ethylenoxid)-metil-metacrylate [$(PEO)_{45}$MEMA] were purchased from Sigma-Aldrich and were used as received. Sodium dodecyl sulfate (SDS), cetyl trimethylammonium bromide (CTAB) and dodecyl trimethylammonium bromide (DTAB) was recrystallized twice from 1:1 benzene and ethanol mixture. Solutions were prepared in ultraclean Milli-Q water (total organic content = 4 ppb; resistivity = 18 mΩ.cm, filtered through a 0.2 μm membrane filter to remove particulate impurities).

II.2. pNIPAm based microgel synthesis

In this study two different methods were used to prepare the microgel particles: the first is based on the method developed by Wu *et al.*[48] and it leads, as previously mentioned, to the preparation of inhomogeneously cross-linked microgel particles; the second method is based on the continuous feeding of the reacting monomers to maintain the constant reaction rate of each component and its development was part of my research. The traditional and the presented new methods will be called batch method and feeding method, respectively.

To help the reader in understanding the preparation of pNIPAm based microgels it is better to state beforehand that pNIPAm microgel particles with different average cross-link densities (XL) have been prepared to better fit the different investigations with the appropriate particle properties. XL is defined as the ratio of the monomer to the cross-linker composing the microgel.

II. 2. 1. Batch method

280 ml Milli-Q water was transferred into the reaction vessel. The temperature of the reactor was set to 80 C (unless it is stated otherwise) and the water was intensively stirred (~1000 rpm). To remove oxygen, nitrogen gas was purged through the reactor for 60 minutes. Calculated amounts of NIPAm monomer and BA cross-linker were dissolved in 18 ml Milli-Q water. To avoid the slow temperature initiated polymerization of the

monomers in the reactor during the initial degassing and heating procedure, the monomer solution was degassed by vacuum at room temperature and injected into the reactor through a septum just before the initiation of the polymerization reaction. After the injection of the monomers 1ml SDS solution was also injected into the reactor then the reaction was initiated by the addition of 1mL APS solution. The solution was stirred intensively during the entire polymerization, while it was continuously purged with nitrogen. In a typical batch pNIPAm synthesis the total monomer concentration was 130 mM, the SDS concentration was 0.65 mM and the APS concentration was 1.2 mM in the reactor.

Negatively charged pNIPA-co-AAc microgel were prepared following the same procedure and by injecting 1 ml of 13 mM AAc into the reactor just before the APS initiator to avoid its volatilization.

For the preparation of the core-shell structured PEO-p(NIPA-co-AAc) microgel particles a batch synthesis was conducted as described above. Moreover in this case 6.5 mM of PEO were added to the reaction mixture after 20 minutes from the initiation of the synthesis.

The pNIPAm based microgels were purified from unreacted monomers and surfactant dialysis against distilled water for 4 weeks.

II. 2. 2. Continuous monomer feeding method

The preparation for the fed pNIPAm synthesis was done similarly to the batch synthesis; that is 280 ml Milli-Q water was transferred into the reaction vessel, heated to 80 °C and purged with nitrogen for 60 minutes. Calculated amount of monomers were dissolved in 18 ml water, degassed by vacuum and transferred into the reactor with 1 ml SDS just before the initiation (1 ml APS). The total monomer concentration was 13 mM, the SDS concentration was 0.65 mM and the initiator concentration was 1.2 mM in the reactor at the beginning of the reaction. To prepare microgel particles with a homogeneous crosslink density of 20, the ratio of the NIPAm and BA monomers was set to 50 in the reactor (for details see *Results and Discussion*). One minute after the initiation of the polymerization the feeding of NIPAm and BA monomers to the reaction mixture was turned on. To make monomer feeding possible the monomers were dissolved in water. The total monomer concentration of the feeding solution was 1.364 mol/dm^3 and the ratio of the NIPAm and BA monomers was 20 in the feeding solution. The solution was degassed, filled into a 60 ml syringe and a total volume of 28.6 ml was fed into the reaction mixture with a feeding rate of 200 μl/min by means of a syringe pump (NewEra Pump Systems, NE-4000). After 143 minutes the feeding

was stopped and the reaction was quenched by switching the temperature of the water circulated in the outer shell of the reactor from 80 to 15 °C.

II.3 Characterization methods

II.3.1. Dynamic light scattering

The dynamic light scattering measurements were performed by means of a Brookhaven dynamic light scattering equipment consisting of a BI-200SM goniometer and a BI-9000AT digital correlator. An argon-ion laser (Omnichrome, model 543) operating at 488 nm wavelength and emitting vertically polarized light was used as the light source. The signal analyser was used in the real-time "multi tau" mode. In this mode the time axis was logarithmically spaced over a time interval ranging from 0.1 μs to 0.1 s and the correlator used 218 time channels. The pinhole was 100 μm. The nanogel samples were cleaned of dust particles by filtering through a 0.8 μm pore-size sintered glass filter.

In the dynamic light scattering experiments the intensity-intensity autocorrelation function was measured (homodyne method) and was converted into the normalized electric field autocorrelation function g by means of the Siegert relation. $g(q, \tau)$ is related to the distribution of the relaxation rate $G(\Gamma)$ through a Laplace transformation:

$$g(q,\tau) = \int_0^\infty G(q,\Gamma)\exp(-\Gamma\tau)d\Gamma \qquad (11)$$

where Γ is the relaxation rate, $q=(4\pi n/\lambda_o)\sin(\theta/2)$ is the scattering vector in which n is the refractive index of the solution, λ_o is the wavelength of the incident light in vacuum and θ is the scattering angle. Since the recovery of $G(\Gamma)$ from the experimentally determined g is an ill-posed problem, several numerical methods have been developed for the analysis of the measured autocorrelation function. In this work we used the cumulant expansion, which gives reliable results in the case of narrow distribution of Γ. This method has the advantage of getting $<\Gamma(q)>$ and $p=\int(\Gamma- <\Gamma(q)>)^2\ G(\Gamma)d\Gamma$ (the so-called first and second cumulants) without any knowledge about $G(\Gamma)$. The first cumulant refers to the mean and the second relates to the width of the relaxation time distribution (polydispersity).

If the intensity fluctuation of the scattered light is due to the translational motion of the particles the collective diffusion coefficient D_m can be calculated from the mean relaxation rate as

$$D_m = <\Gamma> / q^2 = D_o(1 + kc) \tag{12}$$

where c is the concentration of the particles. In case of spherical particles D_o is related to the hydrodynamic diameter of the particles d through the Stokes-Einstein relation:

$$D_o = \frac{kT}{3\pi\eta d} \tag{13}$$

where k is the Boltzmann constant, T is the temperature and η is the viscosity of the medium.

II.3.2. Electroforetic mobility measurements

Malvern Zetasizer NanoZ equipment from Malvern Instruments was used to measure the electrophoretic mobility of the PEI/SDS complexes at different pH values. The instrument uses a combination of laser Doppler velocimetry and phase analysis light scattering (PALS) in a technique called M3-PALS. Prior to the measurements the instrument was always tested with Malvern Zeta Potential Transfer Standard. All the measurements were performed at 25 ^{o}C. The standard error in the values of the electrophoretic mobility was found to be around 10%.

II.3.3. Determination of surfactant binding isother

2 g polyvinyl chloride (M_w=1x10^5) was dissolved in 50 cm^3 THF. 20 cm^3 of this solution, 40 cm^3 THF and 2.97 g tritolyl phosphate was used as membrane forming solution. It was poured on a clean flat glass surface and dried for two days at 40 ^{o}C. The membranes was conditioned in 1 mM CTAB solution for a day then washed out with distilled water. A piece of membrane was placed in a plastic membrane holder[87]. The response time of the membrane was dependent on its thickness. The thick membranes were of slow answer, the very thin ones could easily hurt when managed. The optimal thickness of the membrane was found to be 0.3-0.5 mm. Ones a peace of membrane was successfully prepared and fixed in the holder the electrode worked for long time. The response time of the electrode was within 1-3 minutes depending on the measured concentration range.

The EMF values of the

$$\text{Ag/AgBr/ 0.1M NaBr /membrane/}c_{latex}, c_{CTAB}\text{/Ag/AgBr}$$

galvanic cell were determined by means of a Radelkis research pH-meter at 25.00 ± 0.1 °C. 10 cm^3 c_{latex} nanogel latex solution was placed into the measuring cell and titrated with a CTAB stock solution (of the same latex concentration). The equilibrium EMF values were read at each titration step. The EMF values were converted into surfactant monomer concentration (c_e) by means of a calibration curve. The EMF vs. $\log c_{CTAB}$ function was found to be linear up to the cmc (with a slope of 54 mV) if there was no latex in the solution.

The binding isotherm of the surfactant on the nanogel $B(c_e)$ was calculated from the expression

$$c = c_e + Bc_{latex} + c_{mic} \tag{14}$$

where c and c_e are the total and equilibrium monomer surfactant concentration, respectively, c_{mic} is the concentration of the micelles in monomer unit and c_{latex} is the nanogel latex concentration. The c-c_e difference gives the sum of the micelle concentration and bound surfactant concentration. The calculation of the binding isotherm was restricted to the range $c_e < cmc$ when $c_{mic} \approx 0$.

II.3.4. Ellipsometry

A manual nulling photoelectric ellipsometer with a mercury lamp (546.1 nm) (Type 43702-200E, Rudolph Research Analytical, NJ, USA) was used to determine the thickness of the cellulose films. The ellipsometrical delta (D) and psi (c) values were collected, and the thickness of the films were determined by fitting the measured data to a three-layer optical model: silicon/cellulose/air. On the basis of an earlier work, the cellulose and silicon were assumed to have refractive indices of 1.55 and 3.85, respectively. Although, this procedure leads to slightly incorrect values with respect to the absolute film thickness, it gives a quick and precise determination of the relative film thicknesses. Before the cellulose films were considered, the thickness of the native silicon oxide layer and the anchoring polyelectrolyte, PEI, was measured and they were found to be constant below 4 nm and thus was assumed to be negligible in the calculation of the cellulose layer thickness. An individual sample was prepared in the case of each investigated layer number and for each substrate studied, at least three points were measured to obtain an average film thickness and to determine the film homogeneity.

II.3.5. QCM-D

The formation of the multilayers was studied using a quartz crystal microbalance with dissipation (QCM-D) from QSense AB, Vastra Frolunda, Sweden. The experiments were performed using the Q-Sense E4-instrument, which is designed for controlled flow measurements. The QCM-D measures simultaneously the changes in frequency and dissipation (frictional losses due to viscoelastic properties of the adsorbed layer) at the fundamental resonance frequency, 5 MHz, and its overtones 15, 25, 35, 45, 55, and 75 MHz. For densely adsorbed layers, the frequency change, Δf, is directly proportional to the mass oscillating with the crystal, Δm, according to the Sauerbrey equation:

$$\Delta m = \frac{-\Delta f}{nC} \tag{15}$$

where C is the mass-sensitivity constant (5.72 m2 Hz mg_1 at f0 ¼ 5 MHz) and n is the overtone number. The dissipation factor (D) provides a measure of the energy loss in the system. Adsorption and desorption as well as structural changes may lead to changes in dissipation. Generally, flat or/and rigid structures have a minimal effect on the dissipation, whereas the thick, porous and/or flexible structures increase the dissipation.

II.3.6. AFM

To characterize the film morphology and surface roughness of the multilayer films, AFM imaging was performed using a Nanoscope IIIa AFM (Vecco, Santa Barbara, CA). These images were scanned in tapping mode under ambient air conditions (23 _C and 50% relative humidity). RTESP silica cantilevers (Veeco, Santa Barbara, CA), each with a tip radius of 8 nm and spring constant of 40 N m^{-1} (values provided by manufacturer) were oscillated at their fundamental resonance frequencies, which ranged between 200 and 400 kHz. No image processing except flattening was utilized.

II.3.7. Dye release studies

The loading of microgel multilayers was achieved by immersing the prepared thin film into 2 ml 1.3 × 10^{-4} M aqueous FITC solution at room temperature (~25 °C) for 12 h. Since FITC is sensitive to oxygen, the solution was prepared in degassed water and the dye loading was done in N_2 atmosphere. The release of the dye was studied at room temperature by immersing the FITC loaded multilayers into 2 ml degassed Milli- Q water in N_2 atmosphere. The release was performed in a UV-VIS cuvette and the dye loaded film (10 ×

20 mm) was fully immersed into the release medium. After a certain time the multilayer covered silica slide was moved into another cuvette that was also filled with 2 ml degassed Milli-Q water. This procedure was repeated until the total release time has reached 320 min. The amount of the released dye was determined by measuring the UV-VIS absorbance of the dye at a wavelength of 476 nm after each release step. Thermally induced release was also conducted by immersing the thin film layer into 2 ml degassed Milli-Q water in a 50 °C hot bath. After 10 min the slide was removed from the release medium and placed into another cuvette containing 2 ml room temperature Milli-Q water. The film was allowed to reswell at room temperature for 10 min then the cuvette was placed into the 50 °C hot bath for 10 min. This procedure was repeated for several times until further dye release could not be detected. The amount of the released dye was also determined by measuring the UV-VIS absorbance of the dye at a wavelength of 476 nm after each release step.

II.3.8. Monomer conversion measurements, HPLC

Monomer conversion was measured by HPLC using an apparatus that consisted of a C18 column, a Gilson 305 piston pump and a Gilson 805 manometric module, a Model 7125 Rheodyne injector equiped with a 25 µl sample loop, and an LKB Bromma 2141 variable wavelength detector operating at a wavelength of 224 nm. The HPLC system was coupled with a computer equipped with the Data Apex Clarity software package. A mixture of 30% Milli-Q water and a 70% methanol was used as mobile phase.

To follow the monomer conversion 3 ml samples were taken regularly from the reaction mixture. Sampling was done by sucking the reaction mixture directly into a syringe that was previously filled with 3 ml 10 mM methyl hydroquinone to ensure the immediate quenching of the polymerization reaction in the sample. The unreacted monomers were separated from the polymeric reaction products by using Amicon Ultra-4 centrifugal filter devices containing regenerated cellulose membranes with 3kDa molecular weight cut off. Centrifugation was done in a Hettich 220R centrifuge at 6000 rpm. Prior to their use the membranes were soaked in Milli-Q water to remove traces of glycerine contained by the membrane. It should be noted that in order to avoid the dilution of the separated monomer solution caused by the small amount of water contained in the dead volume of the filtration device the first few hundred microliter filtrate was discarded and only the following filtrate was used for the HPLC measurements. Monomer conversion was determined from at least three parallel measurements with standard deviation smaller than 1%.

III. RESULTS AND DISCUSSIONS

The results and discussions section is divided into three parts. In the first part the preparation of multilayer thin films using responsive microgel particles and a novel material, microfibrillated cellulose is presented. The multilayer was also loaded with a probe molecule and the release characteristics were investigated. The second part describes the kinetics of microgel particles synthesis and proposes a novel method for the preparation of homogeneously cross-linked pNIPAm microgel particles. The third part is intended to investigate the charged pNIPAm based microgel stability as interacting with oppositely charged surfactant and to work out a method to stabilize the uncharged microgel/surfactant complexes sterically.

III.1. Fluorescein uptake and release by multilayers of responsive nanogel particles and nanofibrillated cellulose

As it has been summarized before, the loading and release characteristics of the microgel multilayers are considerably hindered due to the interpenetration of the oppositely charged polyelectrolyte and microgel particles. To overcome this problem, the interdigitation of the oppositely charged polyelectrolytes should be prevented, which seems to be in contradiction with the very nature of the LbL deposition technique[88]. A potential solution to this challenge could be the application of inflexible macromolecules or colloids in the multilayer build-up to evoke charge reversal.

In the present study, the possibility of creating a multilayer using only charge-stabilized colloidal MFC and microgel particles is presented as well as the ability of the multilayer to load and release small molecules (e.g. fluorescein isothiocyanate, isomer I) is investigated. The LbL-assembly was monitored in situ by the quartz crystal microbalance with dissipation (QCMD) technique. Following the assembly, the LbL- morphology was characterized using atomic force microscopy (AFM). The release properties of the FITC-loaded multilayer were determined by measuring the UV-VIS absorbance of the dye. The high aspect ratio, anisotropic and semiflexible nanofibrils are expected to contribute to less interdigitation within the multilayer and, therefore, promote the uptake and release of dye to a significant extent.

III.1.1. Preparation of (pNIPAm-co-AAc) / cationic MFC multilayers

The microgel / cationic MFC multilayers were assembled using the layer by layer deposition approach. The silica surfaces were first exposed to 500 ppm PEI solution for 20 minutes. PEI is a hyperbranched polymer containing primary, secondary, and tertiary amine groups in a 1:2:1 ratio and widespreadly used to functionalize negatively charged surfaces for subsequent LbL deposition. The pH of the PEI solution was not adjusted (pH ≈ 9.5) but its ionic strength was set to 10mM by NaCl. The multilayers were prepared first by exposing the PEI "functionalized" surface to a (pNIPAm-co-AAc) microgel (XL 70) solution (10000 ppm, pH ≈ 7.0 for 20 minutes) and then to a MFC dispersion (1000 ppm, pH ≈ 7.2 for 20 minutes). The deposition steps were repeated until the required layer number had been reached. Each deposition step was followed by four steps of rinsing in water for 5 minutes for the first 3 steps and 10 minutes for the last one. It should be mentioned that the 5 cm long silica strips were always immersed 2 cm deep into the polyelectrolyte solutions and 2.5 cm deep into water, thus insuring formation of multilayers on a well-defined area.

III.1.2. Multilayer structure investigations

Ellipsometry

In order to determine whether the cationic MFC could interact with oppositely charged nanogels to form multilayers, an experiment was conducted where silicon wafers were consecutively treated with the anionic nanogels and cationic MFC using PEI as a pre-cursor layer with thorough rinsing between each step. In the experiment, no extra salt, apart from the 10 mM NaCl during the PEI adsorption, was used. The thickness of the layer formed on the wafers was determined with ellipsometry, and the result is summarized in figure 15. As shown in the figure, the adsorption of the first nanogel layer gives rise to a large increase in layer thickness. However, it should be noted that this increase is much smaller than the diameter of the collapsed gel particles (180nm) measured in the bulk phase by dynamic light scattering. The deposition of additional MFC and nanogel layers results in much smaller further increase of the layer thickness. From the fourth layer the multilayer build-up reaches a steady state, with a similar increase in thickness for each adsorbed nanogel/cationic MFC bilayer.

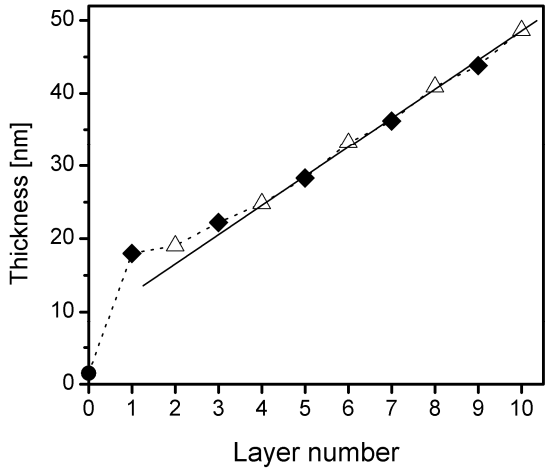

Figure 15. Thickness of a multilayer of nanogels and cationic MFC with PEI as a pre-cursor layer, measured by ellipsometry. The solid diamond (♦) represents the adsorption of the nanogel particles, while the open triangle (Δ) corresponds to the adsorption of the microfibrils. The solid circle (●) denotes the first adsorption step with PEI.

The ellipsometry data clearly indicate the successful build-up of the MFC / nanogel multilayer but the observed thickness increase associated with the formation of a new bilayer (~10nm) seems to be in contradiction with the physical dimension of the microgel beads measured in the bulk phase. To resolve this contradiction we also performed AFM imaging of the prepared multilayers.

AFM

AFM height imaging of the prepared multilayers was recorded in air to determine the morphology of the multilayer films. Amplitude and phase images were recorded to gain additional structural information, as a consequence of variations in the cellulose/nanogel material properties such as adhesion, friction and viscoelasticity. Figure 2a shows representative AFM height and amplitude images of nanogel particles adsorbed to a PEI pre-treated silica surface. The images indicate randomly distributed particles not fully covering the surface. The particles exhibit a narrow size distribution with a particle width of ca. 450 nm. The height of the particles could be determined by imaging a section across two aligned particles. The height was ca. 32 nm and it is obvious that the particles were deformed upon adsorption onto the surface.

Figure 16b, c, e and f show AFM images of a nanogel/cationic MFC bilayer adsorbed onto a PEI pre-treated silica surface. The fibrils can be clearly distinguished, most of them attached

to the gel particles and covering them densely. The microfibrils have a fairly constant width of about 20 nm and appear, as expected, as stiff rods. However, taking into consideration the broadening due to the geometry of the tip, direct measurement of the fibrils in figure 2c shows an average width of 5 nm. This is in good agreement with earlier published TEM micrographs, indicating a microfibril width of about 5 nm for these fibrils that have been modified to contain higher amount of charged groups compared to native fibrils[89,90]. The height of the fibril-embedded particles was ca. 42 nm reflecting a height increase (~10nm) compared to the adsorbed nanogel particles.

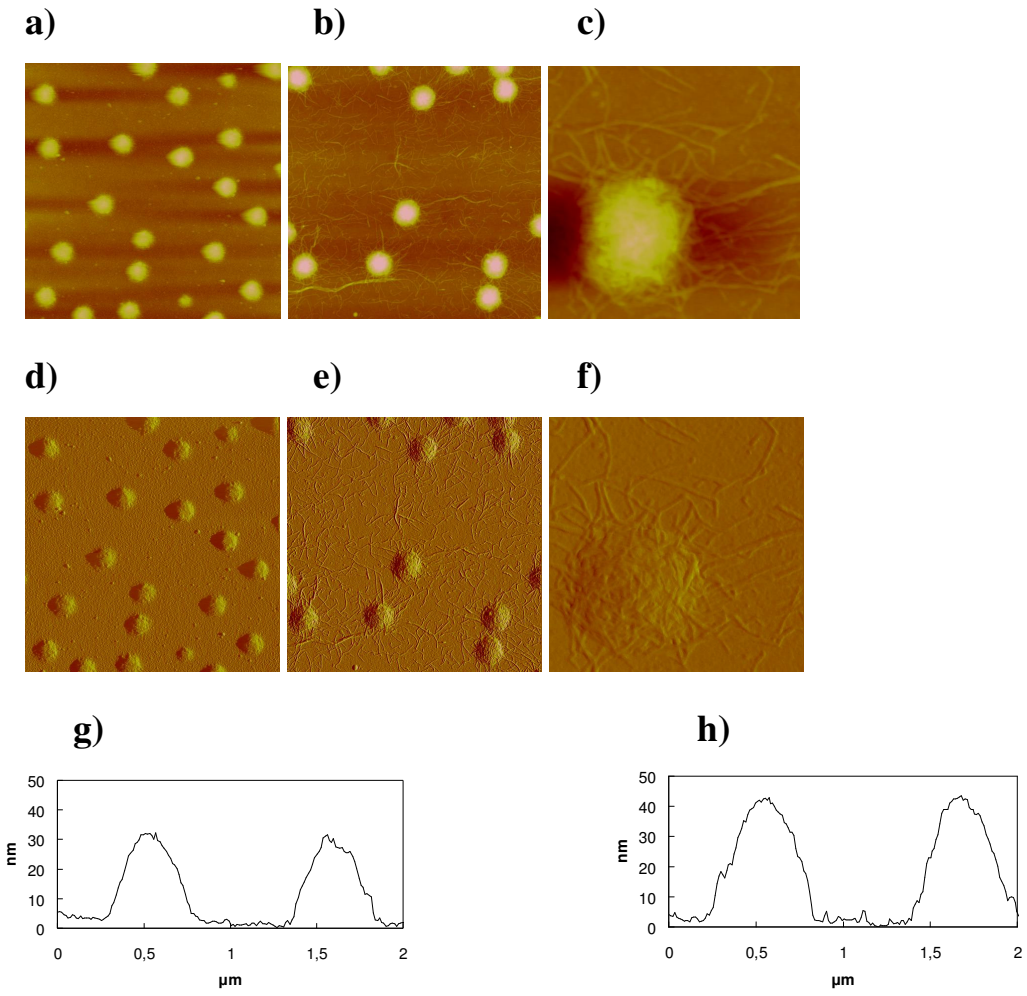

Figure 16. AFM height (a, b, c) and amplitude (d, e, f) images of (a, d) a nanogel monolayer and (b, c, e, f) a nanogel / MFC bilayer adsorbed on a PEI pre-treated silica surface. In (a, b, d, e) the scanned surface area was 5µm x 5µm and the z-range is 65 nm, while in (c, f) they were 1µm x 1µm and 65 nm, respectively. The bottom panels show typical cross sections (g) for the monolayer and (h) for the bilayer.

Figure 17a and b reveals a dense surface structure in the case of a multilayer incorporating 5 bilayers of anionic nanogels/cationic MFC. The surface is considerably rougher than it was observed in the case of a single bilayer and it is fully covered by fibrils. When an additional nanogel layer is adsorbed on top of the fifth MFC layer (figure 3c and d), the nanogel beads provide a uniform but non-dense coverage on the surface. The image seems to reflect that the adsorbing gel particles are localized in the depressions of the rough, MFC covered surface.

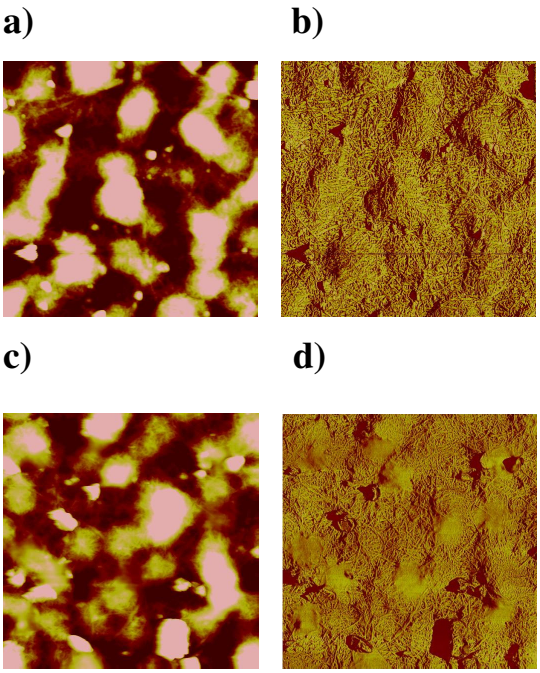

Figure 17. AFM (a) height and (b) amplitude images of MFC terminated 5 bilayers nanogel/cationic MFC multilayer adsorbed onto a PEI pre-treated silica surface. c) AFM height (c) and (d) amplitude image of nanogel terminated 5.5 bilayers nanogel/cationic MFC multilayer. The scanned surface area was 3µm x 3µm in each case and the z-range is 65 nm.

Mechanism of the multilayer build-up

In the first adsorption step of the multilayer build-up the microgel particles bind to the PEI activated substrate. The microgel particles form a disordered monolayer that has an average surface coverage of 0.68 ± 0.08 particles / μm^2. Since both the gel particles and the PEI layer is highly charged at the applied pH (7.0) and the deposition is done in the absence of excess electrolyte, the particle adsorption is expected to be irreversible and rearrangement of the adsorbed particles on the surface is not anticipated. A model used for the description of the irreversible attachment of particles to a substrate is the Random Sequential Adsorption

model (RSA).[38] The RSA model is based on the approach that particles are placed randomly on a surface and their adsorption is accepted if they do not overlap with any previously adsorbed particle. This model predicts 55% maximum surface coverage in the case of non-interacting particles. Assuming that the experimentally found 0.68 particles / μm^2 surface coverage corresponds to the maximum55% surface coverage predicted by the RSA model, the effective diameter of the adsorbing nanogel particles can be estimated as ~1000 nm. The calculated value is in a surprisingly good agreement with the hydrodynamic diameter of the nanogel particles (910 nm) measured in the bulk phase by dynamic light scattering. The observed coincidence of the estimated and the experimental values implies that the surface coverage is primarily governed by the size of the swollen nanogel beads and their irreversible binding on the substrate.

The AFM images measured in the dry state of the nanogel monolayer reveal that the deposited and dried particles are significantly deformed: their height (32 nm) is much smaller, while their horizontal diameter (~400 nm) is much larger than the diameter of a collapsed gel particle in the bulk phase (180 nm). It should also be noted that relaxation towards the non-deformed spherical particle was not observed after a week aging of the samples in the dry state. These observations clearly indicate the rather strong interaction of the adsorbed particles and the underlying polyelectrolyte layer that prevents the in-plane shrinking of the deposited particles. These observations are in good agreement with the results of von Klitzing *et al.*[91], and by in situ AFM swelling studies[92] but seem to be in contradiction with the observations of Vincent *et al.*[93] who found that the film thickness in the dry state was roughly 60% of the collapsed particle size. However, in the latter case the particles were deposited on the substrate in their collapsed state at 10 mM ionic strength, which gave rise to a close-packed monolayer even in the dry state preventing the horizontal swelling, and thus the "spreading" of the particles on the substrate surface.

When the negatively charged nanogel monolayer is exposed to the cationic fibrils, they bind on the surface of the nanogel particles due to the strong electrostatic interaction of the oppositely charged colloids. The fibril-covered dry nanogel particles show an increased height (~ 10nm) that roughly corresponds to the thickness of a few fibrils thick layer. This is in good agreement with the observed high fibril coverage of the nanogel beads, furthermore it clearly indicates that the fibrils do not penetrate inside the gel particles but remain localized on their surface. The accumulation of the cationic MFC on the surface of the gel particles leads to overcharging of the nanogels facilitating the observed multilayer build up.

The uniform surface coverage observed after the deposition of five bilayers indicates that the voids present among the adsorbed particles are filled in during the latter steps of the multilayer build-up. Such a "space-filling" mechanism can insure that the adsorbing nanogel particles can maximize their interactions with the underlying structure. Furthermore, together with the large vertical shrinking of the dry gel particles and the relatively low surface coverage in the individual nanogel adsorption steps, it can also explain the observed rather small thickness increase associated with the formation of a new dry bilayer.

QCM-D

To gain an additional insight into the formation of the nanogel / fibril multilayer, QCM-D measurements were also performed. This investigation allows the *in situ* monitoring of the multilayer formation in its original wet state, thus it can provide further information about the mechanism of the build-up and the structure of the multilayer. Figure 18 shows the layer-by-layer adsorption of nanogels and cationic MFC with PEI as pre-cursor layer, as indicated by the dissipation (Figure 18a) and normalized frequency change (Figure 18b) measured by QCM-D. A stable baseline was first established prior to adsorption of PEI. At time t = 0 min, a finite amount of PEI was injected into the measurement chamber, and a small and rapid decrease in frequency was observed due to the adsorption of the cationic PEI onto the anionic silica substrate. PEI was allowed to adsorb until a steady-state signal was reached. Upon rinsing with Milli-Q water, no significant change in the frequency was observed. At t = 15 min, the rinsing solution was replaced by a colloidal dispersion of nanogels (100 mg/L). A large and distinct decrease in the resonance frequencies was observed, due to the adsorption of the gel beads onto the cationic PEI layer. Once again, free anionic nanogels from the cell were then rinsed away before the multilayer was formed by consecutive treatments with cationic MFC and nanogels. In agreement with the ellipsometry results, the decrease in the third overtone frequency (figure 18c) on each nanogel and MFC injection clearly demonstrates the multilayer build-up, though it has to be noted that the frequency decrease seems to level off from the fourth bilayer.

As shown in figure 18b, the PEI adsorption on the silica substrate gives rise to a small, overtone independent decrease in frequency (~ 5Hz) that is accompanied with a negligible increase in energy dissipation as shown in figure 4a. This is in good agreement with previous QCM-D results[81] and indicates that PEI forms a thin, compact layer on the substrate. The adsorption of the first nanogel layer results in a huge frequency decrease (~80

Hz) compared to the PEI adsorption. The frequency decrease has slight overtone dependence and accompanied with a moderate increase in energy dissipation.

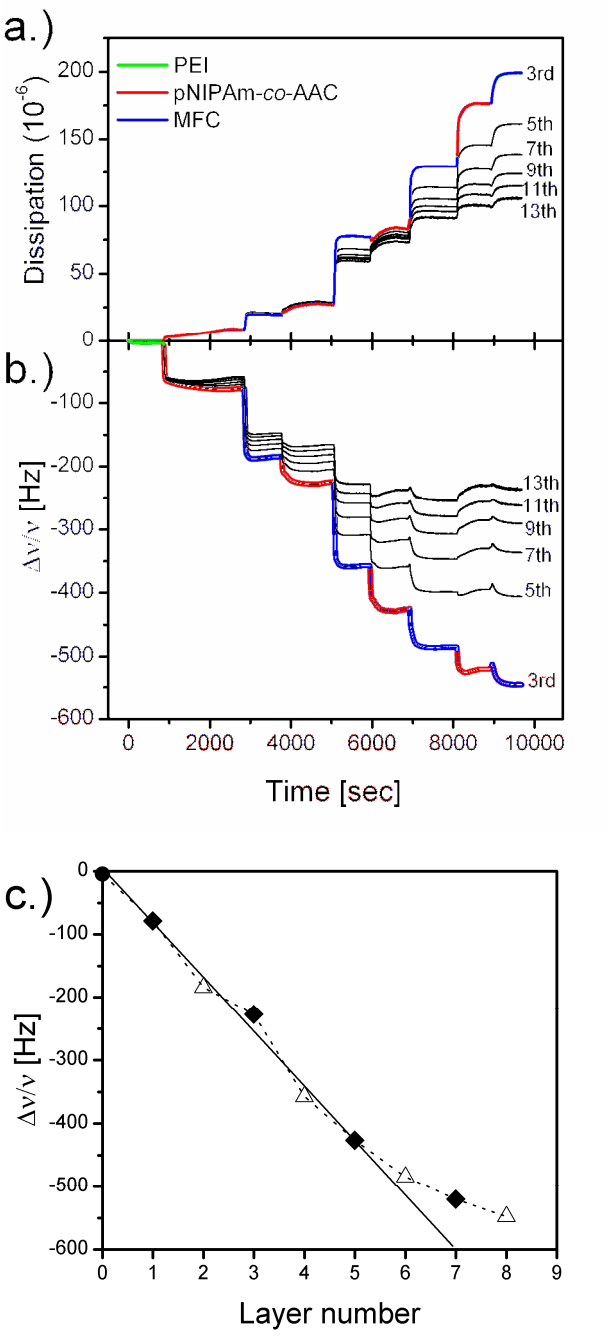

Figure 18. Multilayer formation of nanogels and cationic MFC with PEI as a pre-cursor layer as evaluated by the QCM-D technique. (a) Change in energy dissipation, (b) change in normalized frequency, Δf/ν, as a function of the number of deposited layers. The concentration of the PEI-solution, anionic nanogel and cationic MFC-dispersion was 100 mg/l at pH of 9.5, 7.0 and 7.2 respectively. c) Normalized frequency of the 3rd overtone vs. number of deposited layers. The solid diamond (♦) represents the adsorption of the nanogel particles, while the open triangle (Δ) corresponds to the adsorption of the microfibrils. The solid cicrcle (●) denotes the first adsorption step with PEI.

With additional layer adsorption the spread of overtones increases drastically. As shown in figure 18a, the energy dissipation also shows a steep increase with the layer number. The dissipation increase is governed by the cationic MFC adsorption steps for the first three bilayers. However, for the fourth bilayer the nanogel adsorption also provides a large, overtone dependent dissipation increase. Finally, it should also be noted that the overall magnitude of the dissipation increase is dominated by the third and fourth bilayers where it reaches very high values.

When the dissipation change during the adsorption process reaches a level of about 1×10^{-6} per 10 Hz, the film becomes too soft to function as a fully coupled oscillator[94,95] i.e., the upper parts of the adsorbed layer do not couple elastically to the oscillation of the sensor. This information is revealed by the slope of the dissipation vs. frequency graph, thus it can provide valuable structural insights into the layer formation. Figure 19 depicts the dissipation – frequency curve of the nanogel / MFC multilayer build-up. As it is indicated by the figure, the nanogel deposition gives rise to a rather flat curve during the formation of the first two bilayers. The curve remains similarly flat at the beginning of the third nanogel layer formation but it becomes rather steep by the end of this deposition step. The adsorption of the fourth gel layer is characterized by a steep slope during the whole adsorption process. The sudden change in the slope during the formation of the third gel layer clearly indicates a major structural change in the deposited layer. Figure 19 also reveals that the slope is considerably higher during the MFC deposition than during the previous nanogel deposition in the case of the first two bilayers but from the end of the third gel layer formation it seems to reach a roughly constant high steepness.

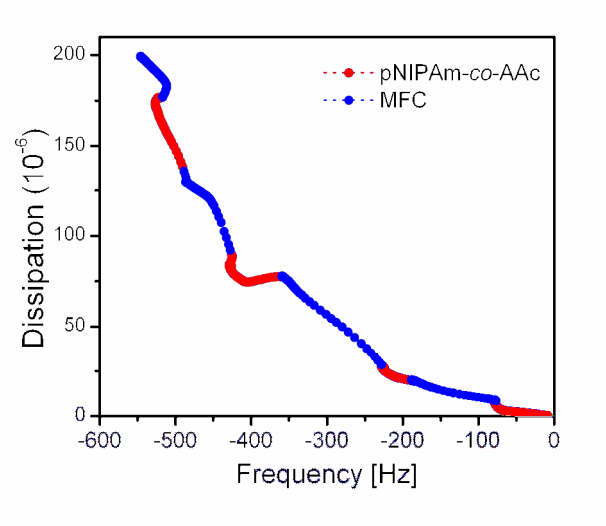

Figure 19. Dissipation vs. normalized frequency for the 3rd overtone as evaluated by the QCM-D technique.

Effect of substrate interaction on the nanogel swelling

As it is revealed by the relatively small overtone dependence of the frequency change and the rather low slope of the dissipation – frequency graph, the nanogel particles adsorbed in the first adsorption step on the PEI layer adopt a rather compact structure. This implies that the gel nanoparticles flatten on the surface even in the wet state, which can be interpreted by the strong interaction and large interdigitation of the oppositely charged PEI and gel segments and by the low crosslink density of the investigated gel particles.

In the subsequent MFC adsorption step the gel particles become densely covered by fibrils as it is demonstrated by the AFM images. Since the fibrils have a length that is considerably larger than the diameter of the adsorbed particles, the microfibrils protrude into the bulk phase from the particle surface. This provides a strong mechanical (viscous) coupling between the adsorption layer and the bulk phase, which is clearly evidenced by the large overtone dependence of the frequency change and the large dissipation increase accompanying all MFC depositions.

The nanogel particles adsorbed in their second and at the beginning of their third adsorption steps seem to retain their compact structure as indicated by the low slope of the dissipation vs. frequency curves. This can be rationalized by realizing that due to the flattening of the adsorbed nanogel particles and their coverage by cationic MFC, the gaps between the already adsorbed nanogels become accessible for new nanogel beads. Taking into account that due to the interdigitation of the oppositely charged segments, the interaction of the PEI and the nanogels is stronger than the interaction of the nanogels and the fibrils, thus the gel particles adsorb mainly on the PEI covered substrate and adopt a flattened structure. However, the situation seems to change drastically during the third nanogel adsorption step. Presumably, when the PEI activated substrate approaches full coverage, the gel particles start to bind in a larger extent on the surface bound fibrils. Since the fibrils cannot penetrate inside the gel particle to form a highly interdigitated structure, the nanogels do not flatten on the surface but preserve their highly swollen state making the layer highly viscoelastic. This is indicated by the leveling off of the third overtone from the third bilayer, by the high spreading of the overtones for both the frequency change and the energy dissipation and by the large steepness of the dissipation vs. frequency curve.

III.1.3. Loading and release characteristics of the nanogel / MFC films

Previous loading and release studies performed on pNIPAm nanogel multilayers indicated that due to the partial collapse of the gel particles triggered by the interdigitation of the oppositely charged polyelectrolyte segments, the room temperature loading and release of the nanogel multilayers is practically negligible[74,96] Since our investigations indicated that the gel particles can retain their highly swollen state in a nanogel / MFC multilayer, we probed this conclusion by investigating the room temperature loading and release of a fluorescent dye (FITC).

Loading of the nanogel thin films with the dye was achieved by immersing the multilayer film into a FITC stock solution ($1.3x10^{-4}$ M) for 12 hours at room temperature. The loaded dye was released by immersing the film into 2 ml Milli-Q water. After a certain time, the multilayer covered substrate was moved into another cuvette containing 2 ml Milli-Q water. This procedure was repeated until the total release time reached 320 minutes. The release experiments were performed as a function of nanogel layer number and the amount of released dye is given as the relative absorbance ($\Sigma A/A_0$) of the dye at 476 nm, where A is the absorbance measured for the released dye and A_0 is the absorbance of the loading solution. Figure 6a shows the cumulative release profiles as a function of the release time for a series of samples prepared with different number of nanogel layers. As seen from the figure, the dye release resembles a saturation type curve that seems to level off during the five hours of the release studies. Actually, it should be noted that the major part of the dye release (~80%) takes place in the first ~20 minutes of the experiment independently of the number of the deposited nanogel layers.

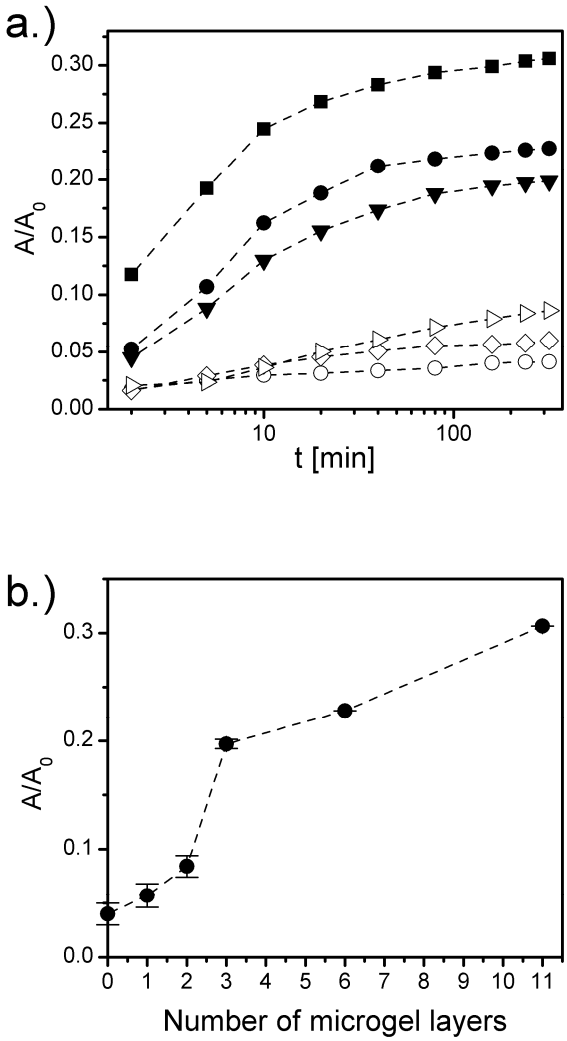

Figure 20. a) Released amount vs. release time at room temperature for a bare PEI layer (open circle), for one (open diamond), two (open triangle), three (solid down triangle), six (solid circle) and eleven (solid square) pNIPAm-*co*-AAc layers, respectively. b) Total released amount vs. number of deposited bilayers.

On the other hand, the overall released amount shows a strong correlation with the number of the deposited nanogel layers. This is depicted in Figure 20b where the overall dye release is plotted as a function of the number of deposited gel layers. A small amount of dye is released even from the bare PEI coated surface. This can be explained by the fact that FITC is a weak acid (pK=6.4), thus it can reversibly bind to the oppositely charged PEI layer. The deposition of one or two layers of nanogel particles on the substrate slightly increases the amount of released dye. However, after the deposition of the third nanogel layer a sudden increase in the released amount can be detected that can be further increased by depositing more nanogel layers. This observation is in very good agreement with the results of the

QCM-D measurements. The initial gel layers that contain highly flattened and strongly interdigitated nanogel particles show a restricted loading compared to the nanogel particles that bind on the MFC covered surface. In the latter case the gel particles remain in their highly swollen state allowing their more effective loading. These results indicate that the nanogel / MFC multilayers form a swollen, open structure that is easily penetrated by small molecules (e.g. drugs).

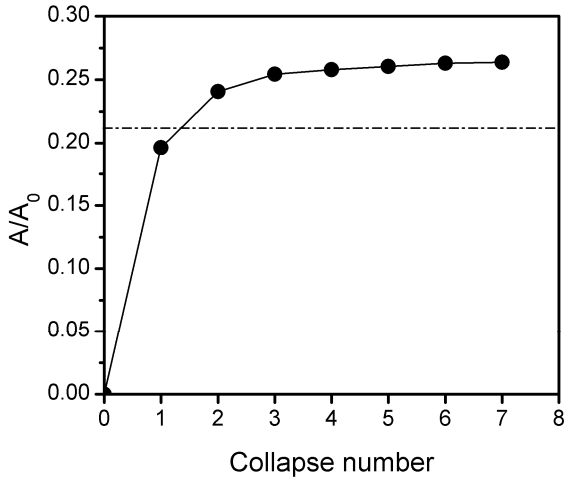

Figure 21. Thermally induced release for six pNIPAm-*co*-AAc layers. The dashed line indicates the maximum amount released at room temperature

Finally, the effect of temperature cycling on the release of the dye was studied. In this experiment we used a multilayer that contained five nanogel layers, and which was loaded using the same room temperature protocol we used in the previous experiments. The release was achieved by immersing the thin film into 2 ml Milli-Q water in a 50 °C hot bath. After 10 minutes the slide was removed from the release medium and placed into another cuvette containing 2ml room temperature Milli-Q water. The film was allowed to reswell at room temperature for 10 minutes then the cuvette was placed into the 50 °C hot bath for another 10 minutes. This procedure was repeated until no further dye release could be detected. The cumulative release profile as a function of the number of temperature cycles are plotted in figure 21. Apparently, a single temperature cycle was enough to release the same amount of dye as in the five hours room temperature experiment. Though, additional temperature cycles can liberate somewhat more dye the first high temperature cycle is responsible for the major part of the release. This result demonstrates that by collapsing the nanogel particles at high temperature they can eject most of their loaded content into the release medium. This behaviour is consistent with a loading / release mechanism where the loaded molecules are

not bound to the multilayer structure but simply the volume of the multilayer structure acts as a reservoir for the probe molecules.

In this investigation it has been shown that LbL-films can be successfully constructed from cationic cellulose I nanofibrils and anionic poly-(N-isopropylacrylamide-*co*-acrylic acid) nanogel beads. AFM tapping-mode imaging of the nanocellulose-based multilayer films showed randomly adsorbed microfibrils with a typical width of about 5 nm covering the nanogel surfaces. *In situ* QCM-D measurements have also revealed that the nanogel beads preserve their soft, gel-like interior that is wrapped by the adsorbed nanofibrils. The lack of the interpenetration of the oppositely charged components gives rise to the formation of an open composite structure that is highly penetrable for other molecules. This was confirmed by investigating the loading and releasing of a fluorescent dye (FTIC). These investigations revealed that the nanogel films could load and release the dye at constant room temperature, which is in contrast to previously reported systems based on synthetic polyelectrolytes. By raising the temperature of the film above the collapse temperature of the nanogel particles a burst release of the dye could also be initiated. Such films may provide a template for controlling loading and release characteristics in future drug release systems (e.g. drug and gene delivery agents), and they can serve as structural materials e.g. in biosensors or in soft actuators.

III.2. Preparation of pNIPAm microgel particles with homogeneous crosslink density distribution

The motivation of our work was to develop a method suitable for the preparation of homogeneously cross-linked pNIPAm microgel particles. To achieve this goal, first we carried out a detailed investigation of the kinetics of the microgel particle formation performed by the traditional preparation method described by Wu *et al.*[48]. As it is summarized in the introduction this method produces close to monodisperse microgels with inhomogeneous cross-linker distribution within the particles.

In the second part of the discussion a new preparation method is proposed for the formation of homogenous microgel particles. This method is based on the continuous feeding of the reacting monomers to maintain the constant reaction rate of each component. In order to distinguish the two preparation methods used in this study, the traditional and the presented new methods will be called batch method and feeding method, respectively.

III.2.1. Batch method

To facilitate the formation of homogenously cross-linked pNIPAm particles, first we addressed how the particle homogeneity is affected by the reaction conditions. In Fig. 22a the total conversion of the monomers, $C_{tot} = 1 - \{c_{NIPAm}(t) + c_{BA}(t)\} / \{c_{NIPAm,t=0} + c_{BA,t=0}\}$, is plotted as a function of the reaction time (t) at different reaction temperatures (θ). The investigated temperatures range, θ = 60-80 ^{o}C, corresponds to typical experimental values used in the literature. As it is indicated by the figure, with increasing temperature the polymerization becomes faster. While at 60 ^{o}C the reaction is completed in approximately two hours, at 80 ^{o}C only about 30 minutes is needed to complete the polymerization. Furthermore, the figure also indicates that with increasing temperature the induction period of the polymerization diminishes on the experimental timescale. This is in agreement with the general expectation that with increasing temperature the decomposition rate of the persulfate initiator should considerably increase.

In Fig. 22b the conversion of the NIPAm monomer ($C_{NIPAm} = 1 - c_{NIPAm}(t) / c_{NIPAm,t=0}$) and the conversion of the BA cross-linker ($C_{BA} = 1 - c_{BA}(t) / c_{BA,t=0}$) are plotted as a function of the total conversion. In this representation the NIPAm conversion is a straight line because $c_{NIPAm} >> c_{BA}$, thus the total conversion is dominated by the conversion of NIPAm monomer ($C_{tot} \approx C_{NIPAm}$). However, the BA conversion shows a positive curvature at each temperature indicating that the BA cross-linker has a larger conversion than the NIPAm monomer

throughout the reaction. This leads to the inhomogeneous cross-link density distribution within the particles as it has been highlighted in the literature. It should be noted that the deviation of the BA conversion curve from linearity (consequently, the inhomogeneity of the microgel particles) increases with decreasing reaction temperature. Therefore, in favour of particle homogeneity we performed all of our microgel preparations at 80°C.

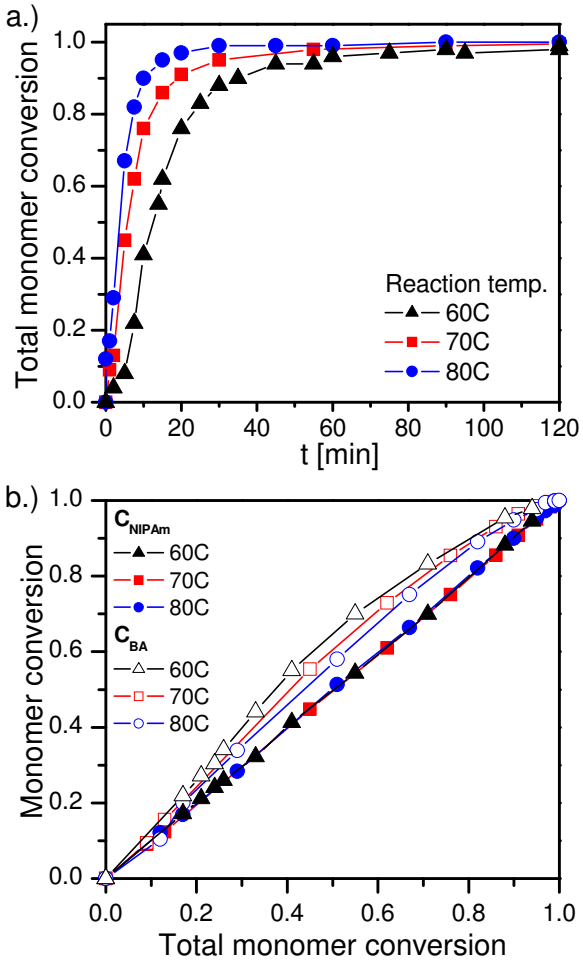

Figure 22. *a)* Total conversion of monomers as a function of reaction time. *b)* The conversion of the NIPAm monomer (solid symbols) and the conversion of the BA cross-linker (open symbols) as a function of total monomer conversion. The synthesis were performed at 60C (black triangle) 70C (red square) and 80C (blue circle), respectively.

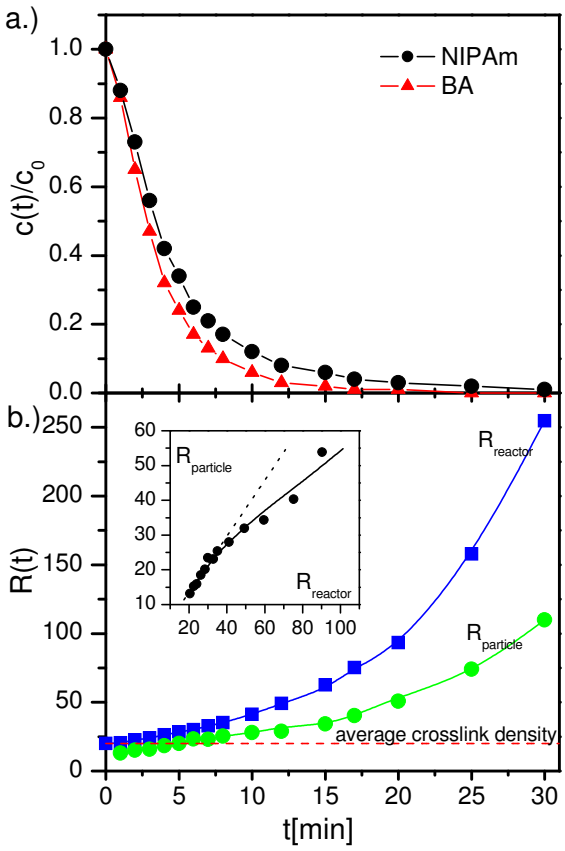

Figure 23. *a)* The relative concentration of the unreacted monomers as a function of reaction time (total monomer concentration: 130mM, θ=80C). *b)* The instantaneous ratio of the monomer concentrations in the reactor ($R_{reactor}$, squares) and $R_{particle}$ (see eq.2 and text; circle) as a function of reaction time. The dashed line indicates the average crosslink density of the microgel particles (the initial monomer ratio). The inset indicates how $R_{particle}$ varies with $R_{reactor}$ during the course of the reaction.

In Fig. 23a the relative concentration ($c(t)/c_0$) of the NIPAm and BA monomers is plotted as a function of the reaction time at 80 °C. As it is shown in the figure, the relative BA concentration decreases faster in the reactor, i.e. the consumption of the BA monomer in the reactor is faster than that of the NIPAm. This has been interpreted in terms of the higher reactivity of the BA monomer. To demonstrate how this affects particle homogeneity, we have calculated the ratio of the instantaneous consumption of the two monomers:

$$R_{particle}(t) = \frac{c_{NIPAm}(t+\Delta) - c_{NIPAm}(t)}{c_{BA}(t+\Delta) - c_{BA}(t)} \qquad (16)$$

This quantity describes the crosslink density of the forming hydrogel at any specific reaction time (t). If we adopt the hypothesis of the inside-out growth[97,98], which assumes that polymerization takes place in the outer shell of the particles because the growing particles are in a compact collapsed state at the reaction temperature, then $R_{particle}(t)$ describes the

radial distribution of the cross-linker within the microgel particles; i.e. the change of the local NIPAm/BA ratio from shell to shell starting from the centre (at the early stage of polymerization) to the periphery of the (completely grown) particle. $R_{particle}(t)$ should be constant if the particles are homogenous.

$R_{particle}(t)$ is calculated for the pNIPAm synthesis performed at 80 ^{o}C and it is plotted in Fig. 23b. At the beginning of the polymerization $R_{particle}$ is much smaller (~10) than the average monomer ratio in the reactor (20) but it rapidly increases with proceeding polymerization. The $R_{particle}$ function indicates that in the center of the gel particles the cross-link density is significantly higher than the average value and the most outer shell of the completely grown particle is practically not cross-linked. In Fig.23b the instantaneous ratio of the unreacted monomer concentrations ($R_{reactor} = c_{NIPAm} / c_{BA}$) is also plotted. As it is indicated in the figure $R_{particle}$ and $R_{reactor}$ seem to change in line with each other implying that the two quantities are not independent. To establish the relation between $R_{particle}$ and $R_{reactor}$, the reaction rate of the two monomers can be written as below, if we assume that the reactivity of the growing polymer chain is not affected significantly by the chemical nature of the last monomer incorporated into it ($k_{Pol\text{-}NIPAm^*/BA} \approx k_{Pol\text{-}BA^*/BA}$ and $k_{Pol\text{-}NIPAm^*/NIPAm} \approx k_{Pol\text{-}BA^*/NIPAm}$, where $k_{Pol\text{-}NIPAm^*/X}$ denotes the rate constant of a NIPAm terminated polymer radical with monomer X and $k_{Pol\text{-}BA^*/X}$ denotes the rate constant of a BA terminated polymer radical with monomer X, respectively and X is either a BA or a NIPAm monomer):

$$\frac{dn_{NIPAm}}{dt}(t) = -k_{NIPAm}[\,Pol^*\,][\,NIPAm\,], \tag{17}$$

$$\frac{dn_{BA}}{dt}(t) = -k_{BA}[\,Pol^*\,][\,BA\,]. \tag{18}$$

The square brackets indicate the equilibrium concentration of the components and Pol^* denotes the polymeric radicals in the reaction mixture. $R_{particle}$ can be defined as the ratio of eqs. 17 and 18:

$$R_{particle}(t) = \frac{dn_{NIPAm}}{dn_{BA}}(t) = \frac{k_{NIPAm}}{k_{BA}}\frac{[\,NIPAm\,]}{[\,BA\,]} = \frac{k_{NIPAm}}{k_{BA}}R_{reactor}(t). \tag{19}$$

Thus, eq.19 indicates that there is simple linear relationship between the instantaneous ratio of the unreacted monomer concentrations in the reaction mixture ($R_{reactor}$) and the crosslink density of the instantaneously forming hydrogel ($R_{particle}$). In the inset of Fig.23b, $R_{particle}$ is plotted as a function of $R_{reactor}$. As it is indicated in the figure the linear relationship indeed holds for a while during the reaction, however at higher conversions a slight deviation can be observed from the linearity indicating that at high conversion the consumption of the BA

cross-linker became even more favoured. This indicates that the assumptions used in the derivation of eq.19 are not strictly valid, though they can be a good approximation. Eq.19 has an important implication regarding the particle inhomogeneity. It suggests that the particle inhomogeneity is only an indirect consequence of the different monomer reactivities, the direct cause is the continuous change of the monomer ratio in the reactor. Thus, if $R_{reactor}$ is kept at a constant value during the polymerization then it can be expected that $R_{particle}$ will also be constant, i.e. homogeneous particles can be produced.

III.2.2. Feeding method

In principle a constant $R_{reactor}$ value can be ensured by appropriate feeding of the monomers into the reactor during the polymerization reaction. Technically the simplest approach is the continuous replacement of the reacted monomers during the polymerization, thus keeping the absolute monomer concentrations constant in the reaction mixture. However, this means that the polymerization must be stopped abruptly at the end of the reaction (e.g. by the rapid cooling of the reaction mixture), otherwise the synthesis would be completed by the formation of an inhomogeneous outer shell around the gel particles as in the case of the batch method. Furthermore, it is desirable to reduce significantly the initial monomer concentration because the final reaction mixture contains the same amount of monomers as the initial one giving rise to a poor reaction yield. For this reason we decided to reduce the initial monomer concentration in the reactor by an order of magnitude (from 130 mM to 13 mM).

To prepare homogeneously cross-linked microgels two important parameters has to be determined. One parameter is what value of the free monomer ratio in the reactor ($R_{reactor}$) gives rise to a desired crosslink density ($R_{particle}$) value in the microgel particles. The other parameter is what the reaction rates of the monomers are at the applied reaction condition, so the monomers can be fed with an appropriate rate into the reaction mixture to ensure constant monomer concentrations during the reaction. To determine these parameters we performed a series of batch pNIPAm synthesis. The total monomer concentration was decreased to 13 mM and the average crosslink density (the initial monomer ratio in the reactor, $R_{reactor,0}$) was varied from 15 to 50. The decreased monomer concentration had two important consequences. As it is expected (see Eqs. 17 and 18) the rate of the polymerization reaction (the monomer consumption) became slower. However, the reaction rate decreased for the NIPAm monomer in a larger extent, thus the synthesis performed at lower total monomer concentration gave rise to even more inhomogeneous microgel

particles than in the case the original synthesis (data are not shown). This observation is in agreement with our previous result, what showed that at high monomers conversion (low monomer concentration) the consumption of the BA cross-linker became more favoured (see the inset of Fig.23b).

To establish the relationship between the ratio of the monomer concentrations in the reactor ($R_{reactor,}$) and the crosslink density of the instantaneously forming hydrogel ($R_{particle}$) both quantities were determined for each of the performed microgels synthesis. The results are summarized in Fig.24. As it is indicated by the figure the ratio of the incorporation rate of the NIPAm and BA monomers ($R_{particle}$) is a linear function of the actual monomer ratio in the reactor ($R_{reactor}=c_{NIPAm}(t)/c_{BA}(t)$) independently of the initial monomer ratio used in the reaction and the extent of the monomer conversion. Thus, it can be concluded that when the polymerization is conducted at low monomer concentrations (< 13mM) eq. 19 provides a reliable relationship between the instantaneous composition of the reaction mixture ($R_{reactor}$) and the crosslink density of the instantaneously forming hydrogel ($R_{particle}$). This means that by controlling the composition of the reaction mixture we should be able to control the crosslink density of the forming microgel particles.

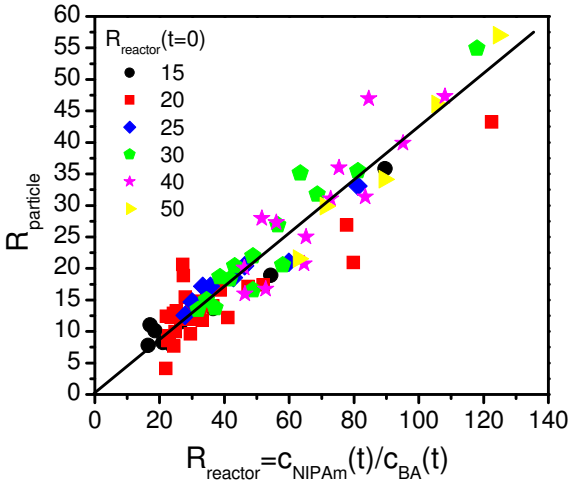

Figure 24. $R_{particle}$ vs. $R_{reactor}$ relationship determined for a series microgel synthesis performed with different initial ratio of the NIPAm and BA monomers (total monomer concentration: 13mM, θ=80C).

The monomer conversion vs. reaction time data (not shown here) also allowed the determination of the initial rate of the monomer conversion. The initial conversion rate of the NIPAm monomer was found practically independent of the initial monomer ratio in the reactor ($0.86 mM \cdot dm^{-3} min^{-1}$), since the initial NIPAm concentration was practically identical with total monomer concentration in each case due to the more than order of magnitude

smaller BA concentrations. On the other hand, the corresponding initial conversion rates of the BA monomer could be well described by eq.19 as a function of the initial monomer ratio ($R_{reactor,t=0}$) and the NIPAm conversion rate.

Finally, to test the formation of the homogenously cross-linked pNIPAm particles we performed a microgel synthesis using the feeding method. The crosslink density of the synthesized particles ($R_{particle}$) was chosen to be 20. Based on Fig.24 the initial monomer ratio was set to 50 in the reactor to produce particles with a crosslink density of 20 and the monomer ratio was set to 20 in the fed monomer solution. The total amount of the fed polymer was identical to the amount of monomers used in the batch synthesis and the feeding rate was set to match the experimentally determined initial monomer consumption rates (0.90mM·dm^{-3}min^{-1} for the 20:1 mixture of the NIPAm and BA monomers; for further details see the experimental section).

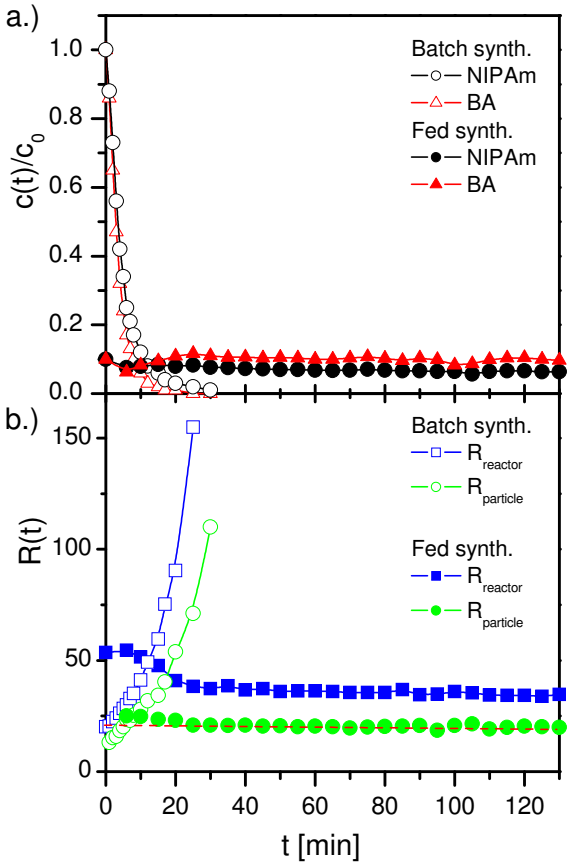

Figure 25. *a)* The concentration of the monomers in the reactor normalized by their total amount polymerized in the reaction as a function of reaction time (θ=80C). *b)* The instantaneous ratio of the monomer concentrations in the reactor ($R_{reactor}$, blue squares) and $R_{particle}$ (see eq.2 and text; green circle) as a function of reaction time. The red dashed line indicates the average crosslink density of the microgel particles (the initial monomer ratio). The open symbols present the results of the batch synthesis, while the solid symbols present the results for the feeding method.

The results of the batch and the feeding methods are compared in Fig.25. As it is demonstrated in the figure while the monomer concentrations steeply decreased in the case of the batch method as a function of the reaction time, in the case of the feeding method following a slight variation at the beginning of the reaction the monomer concentrations adapted practically constant values. As a consequence the monomer ratios showed slight changes at the beginning of the reaction both in the reactor ($R_{reactor}$) and in the case of the consumed monomers ($R_{particle}$) but stabilized afterwards, which is in sharp contrast with the batch synthesis where the monomer ratios diverged as a function of reaction time. The slight initial variation of the instantaneous cross-link density of the microgels in the case of the feeding method is likely due to a small error in the experimentally determined feeding rates of the monomers or the initial crosslink density used in the reactor. However, the fact that the monomer concentrations, and thus the instantaneous crosslink density of the particles quickly converged to steady-state values, clearly demonstrate the robustness of the applied method for the preparation of microgel particles with homogenous internal structure.

III.2.3. Latex optical properties

The optical appearance of the microgel latexes synthesized by the two different methods is very different. This is demonstrated in Fig. 26a, where the picture of 0.1w% latexes can be seen at room temperature. The pNIPAm latex synthesized by the batch method is highly turbid, while the latex prepared with the feeding method is practically transparent. The turbidity of a colloid system is determined by two major factors. One is the scattering contrast (the refractive index difference of the particles and the surrounding medium), while the other one is the size of the particles.

To separate these effects we performed dynamic light scattering (DLS) measurements on the prepared samples. Fig. 26b shows the hydrodynamic diameter of microgel particles as a function of sample temperature. Both samples show the temperature dependent swelling of the pNIPAm microgels. The collapse temperature of the microgels is practically unaffected by the microgel preparation method, which is in agreement with previous experimental results that indicated similar collapse temperatures for pNIPAm macro- and microgels independently of their crosslink density[99]. The hydrodynamic diameter of the pNIPAm particles prepared by the feeding method is larger in the entire investigated temperature range. Since the turbidity of a colloid system significantly increases with the increasing particle size, the lower turbidity of the larger microgel particles can be explained only with their much smaller scattering contrast. This can be rationalized in terms of the different

internal structure of the microgel particles prepared with the different techniques. In the case of the batch method the core of the microgel particles has a much larger crosslink density, which hinders the swelling of the particle core and results in significant refractive index difference between the particle core and the solution phase even in the swollen state. At the same time the microgel particles prepared by the feeding method exhibit a homogenous crosslink density distribution within the particle, thus it can swell uniformly, which gives rise to the small scattering contrast of the swollen particles and low turbidity of the latex. In agreement with this interpretation Fig. 26b also indicates that the microgels prepared by the feeding method show much larger swelling at room temperature ($V_{25}/V_{40,Feeding}$ = 13.9 and $V_{25}/V_{40,Batch}$ = 6.7).

The DLS measurements have also indicated that the pNIPAm particles are highly monodisperse (p=0.02±0.02) independently of the temperature and the preparation method. The monodispersity of the particles is also demonstrated in Fig. 26c. It is well established in the literature that monodisperse soft particles can be packed in ordered closed packed structures e.g. by centrifugation[100] which is evidenced by the iridescent colours of the samples. Fig. 26c shows that the microgel samples form opaque, iridescent samples after centrifugation at 40°C independently of the method of preparation. On the other hand the iridescent colours, observed for the different samples, are significantly different. The microgels prepared by the batch method produce green-blue colour, while the microgels prepared by the feeding method are dominantly red. Since the observed colour can be interpreted as the result of light diffraction from the ordered colloidal arrays having a lattice spacing on the order of visible light, the observed colour difference is related to the larger size of the microgels produced with the feeding method.

It is interesting to note that if centrifugation is performed at room temperature (Fig. 26d) then the optical properties of the formed closed packed structures change very differently for the two different microgel preparations. In the case of the batch method a significant red shift of the iridescent colour can be observed, but the opaque character of the sample does not change. At the same time in the case of the feeding method a colourless, completely transparent system is formed. These differences are related to the different internal structure of the synthesized microgels. In the case of the batch method the inhomogeneous internal structure of the microgels gives rise to a high scattering contrast even in the swollen state as explained before and results in opaque samples, which show a red shift of the iridescent colour with decreasing temperature due to the swelling of the particles.

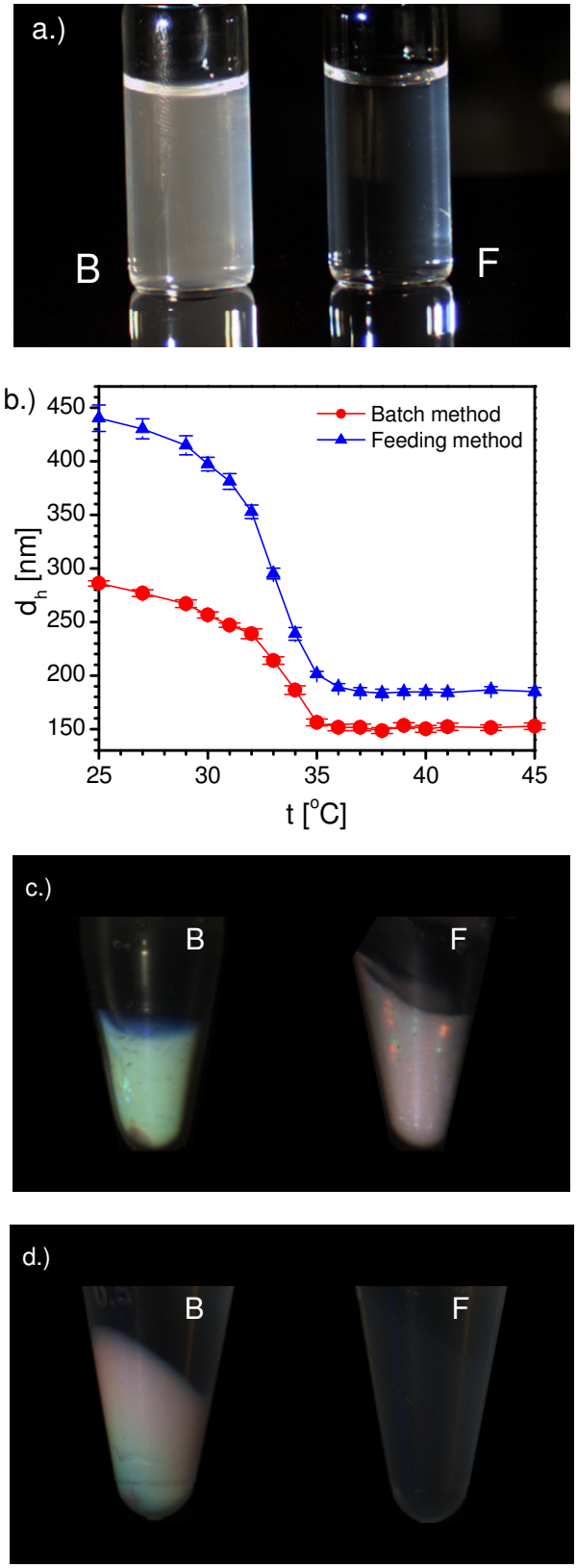

Figure 26. *a)* 0.1 w% pNIPAm samples at room temperature. *b)* Hydrodynamic diameter of the microgels as a function of temperature. *c)* pNIPAm samples centrifuged at 40C and *d)* at 25C to form colloid crystals. 'B' denotes samples prepared by the batch method, while 'F' denotes samples prepared by the feeding method. The samples have identical crosslink density.

At the same time the homogenous internal structure of the microgels prepared by the feeding method have a very low scattering contrast in their swollen state because of their uniformly swollen, water rich structure. The low scattering contrast and the large size of the swollen particles explain the formation of the transparent and colourless close packed samples in this case.

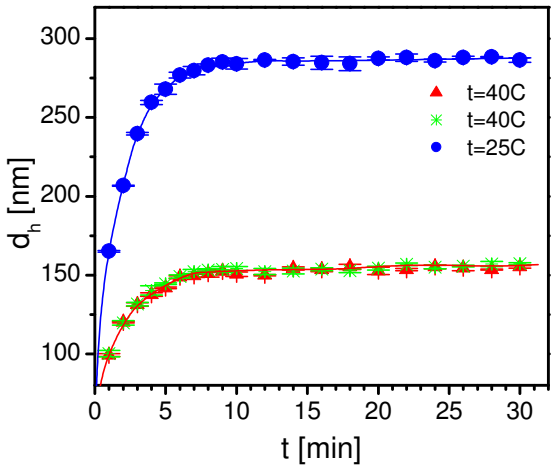

Figure 27. The hydrodynamic diameter of the microgel particles as a function of reaction time in the case of the batch polymerization. The stars denote data points that were measured by cooling the sample from the reaction temperature (80°C) to the temperature of the DLS measurement (40°C). Triangles are data points that were measured on samples purified at room temperature by repeated centrifugation and redispersion, then measured at 40°C. Circles represent data points that were measured at 25°C on purified samples. The lines are guide to the eyes.

III.2 4. Development of the microgel particles

pNIPAm microgel particles form by precipitation polymerization, that is the growing primary polymer chains collapse and aggregate to form the growing polymer particles. The formation of the intact microgel particles requires the crosslinking of the aggregated primary chains. We also investigated the timescale of this process both in the case of the batch polymerization and in the case of the feeding polymerization. The experiment we carried out was that the polymerization was stopped in the samples that were taken from the reaction mixture by methyl hydroquinone but the samples were not allowed to cool below the LCST. The samples were split and the particle size was determined in one set at 40 °C (above the LCST). The other set was cooled to room temperature and purified by repeated centrifugation and redispersion, then the particle size of the purified microgels was determined at 25 and 40 °C.

The results of these measurements are summarized in Fig.27 for the batch polymerization. The presented data clearly indicate that after cooling and reheating, the particles preserve their size in each sample. This means that under the applied reaction conditions (temperature and average crosslink density) the cross-linking of the particle core takes place before the first sample was taken (t=1min). This result is in agreement with the observations of Wu et al.[51] who also found that the particle size was independent of thermal history in the case of similarly cross-linked microgel particles.

The results of a similar experiment for the feeding polymerization are summarized in Fig.28. Since in the case of the feeding polymerization the monomer concentration is kept constant in the reactor the conversion is determined by the amount of fed monomers. Assuming that the microgel particles have a uniform density distribution, the hydrodynamic size of the formed particles can be calculated as a function of reaction time.[1] The calculated diameters are plotted as continuous lines in Fig. 28a. As it is indicated by the figure when the samples were not allowed to cool below the LCST (green stars in Fig. 28) the size of the particles were slightly smaller than the calculated values in the first hour of the reaction. At the same time, these samples were also found slightly polydisperse. With increasing reaction time the experimentally determined particle diameters converged to the calculated values and the polydispersity of the samples gradually decreased. After ~60 minutes the calculated and the measured particle diameters became identical and the samples became highly monodisperse, indicating that the major fraction of the polymer chains is incorporated in the growing microgel particles.

[1] Calculations were done by using the assumptions that the volume of the particles is proportional to the amount of the NIPAM monomers built in the particles ($V = \pi d_h^3/6 \propto 1\text{-}c_{NIPAm}/c_{o,NIPAm}$) and that convertion is proportional to the reaction time ($1\text{-}c_{NIPAm}/c_{o,NIPAm} \propto t$). This leads to the equation: $1\text{-}c_{NIPAm}/c_{o,NIPAm}) = k_2\, t^3$ and the unknown k_2 constant was calculated from the d_h value measured by DLS at t=140 minutes (where $c=c_o$).

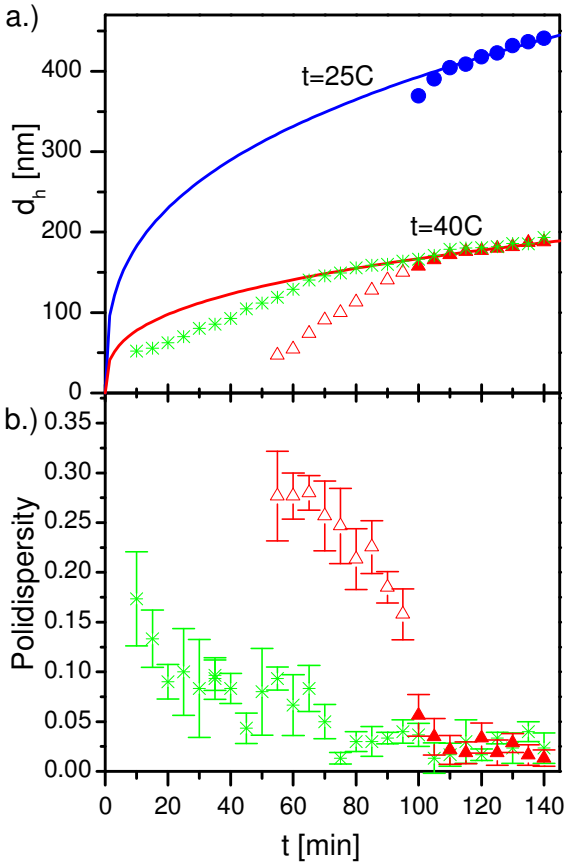

Figure 28. *a)* The hydrodynamic diameter and *b)* the polydispersity of the microgel particles as function of reaction time in the case of the feeding method. The stars denote data points that were measured by cooling the sample directly from the reaction temperature (80°C) to the temperature of the DLS measurement (40°C). Triangles were measured at 40°C, while circles were measured at 25°C for samples that were allowed to cool below the LCST. Solid symbols are data points that were measured on samples purified at room temperature by repeated centrifugation and redispersion. Open symbols denote data point that were measured without purification but were allowed to cool below the LCST, then reheated to 40°C. Lines are calculated hydrodynamic diameters (see text).

When the DLS measurements were repeated on the room temperature purified and reheated samples, the measured particle diameters were found identical with particle sizes measured for the never-cooled samples, when the sampling time was sufficiently long (>100 min). This confirms that by the end of the reaction intact microgel particles form in the feeding polymerization. However, when the sampling time become shorter than ~100 minutes the microgel concentration suddenly sharply dropped in the purified samples and DLS measurements could not be performed. This implies that when the temperature was decreased below the LCST the primary polymer chains could dissolve from the particle in the lack of sufficient cross-linking and the resulting small polymer fragments remained in

the supernatant during the centrifugation. To confirm this conclusion, the DLS measurements were repeated on reheated but non-purified samples (open symbols in Fig.28). These measurements indicated smaller average particle size in the case of the reheated samples and diverging polydispersity. The Contin analysis of the measured autocorrelation functions indicated multimodal distribution in these samples. These observations confirm that the samples taken before 100 minutes reaction time dissolved upon cooling and formed new highly polydisperse, smaller particles when they were reheated.

The above results indicate that in the case of the feeding polymerization the formation of the intact microgel particles requires orders of magnitude longer time than in the case of the batch reaction. Even more importantly the formation of the intact microgels occurs only around 70% conversion in the case of the feeding reaction, while in the case of the batch reaction this happens at lower than ~20% conversion. These differences are presumably related to the much higher cross-linker concentration in the initial core of the microgel particle in the case of the batch synthesis, which facilitates the interchain cross-linking of the aggregated primary polymer chains.

Finally, we have also determined how the swelling of the microgel particles evolve during the particle growth. To characterize microgel swelling, the ratio of the volumes of the swollen particle (25 °C) and the collapsed particle (40 °C) were calculated using the particle sizes determined by DLS (Figs. 27 and 28). The calculated swelling ratios are plotted in Fig. 29 as a function of collapsed particle size for both the batch and the feeding polymerizations. For the batch synthesis the swelling increases with increasing particle size then shows a maximum at large conversions, which is followed by a small drop as the particle size slightly increases further. These observations are in agreement with the results of Wu et al..[51] The initial increase in swelling indicates the decreasing crosslink density of the outer shells of the particle, while the final drop in swelling was attributed to the increased crosslinking at the end of the reaction due to the consumption of the pending double bonds within the particle. If the swelling of the microgel particles prepared by the feeding method is compared to the swelling of the particles prepared by the batch method, two main differences can be identified. First, the swelling of these particles is much larger despite of the equal average crosslink density used in the two microgel preparations; second the swelling is independent of the particle size (conversion) after the formation of the intact microgel particles. Both differences indicate that the particles prepared by the feeding method have a different internal structure. The swelling results (large, size independent

swelling) are in good agreement with the uniformly cross-linked, homogenous internal particle structure that is also implied by the kinetic measurements and the optical properties of the formed particles.

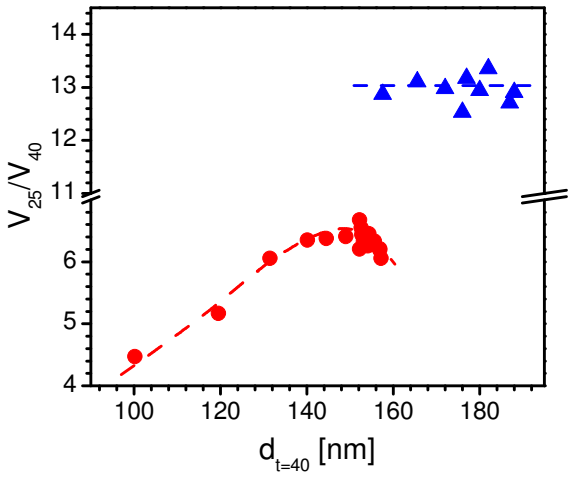

Figure 29. The swelling ratio of the microgel particles as a function of the collapsed particle size. Triangles were measured for samples prepared by the feeding method and the circles were measured for samples prepared by the batch method. The dashed lines are guides to the eyes.

III.3. Preparation of sterically stabilized complexes of oppositely charged microgels and surfactants

An important family of drug carrier complexes is formed by the association of oppositely charged macromolecules and actives. Though, the potential application of these complexes range from gene delivery to controlled insulin release, there are two major problems associated with their application: close to stoichiometric mixing these complexes loose their colloid stability due to charge compensation, which leads to the aggregation and precipitation of the formed complexes; far from stoichiometric mixing they form electrostatically stabilized complexes that are sensitive to high ionic strength and that usually trigger immune response due to their charged nature.

The goal of this investigation was to develop a new family of sterically stabilized microgel particles, which can preserve their colloid stability even at stoichiometic mixing and which have an enhanced biocompatility. Furthermore, we aimed at the application of a novel synthetic approach that allowed the preparation of the protective outer shell and the charged core of the particles in the same synthetic step. To characterize the colloid stability of the complexes formed by the p(NIPAm-co-10%AAc) microgel particles prepared both with and without the protective shell, we have investigated the interaction of cetyl trimethylammonium bromide (a cationic surfactant) and the negatively charged microgels.

III.3.1 Investigation of the p(NIPAm-co-AAc)/CTAB interaction

Determination of the binding isotherm of the surfactant on the polymer is one of the most important thermodynamic measurement that provides information about the nature of surfactant binding. In Fig. 30 the binding isotherm of CTAB on the p(NIPAm-co-AAc) microgel of crosslink density 70 is plotted against the equilibrium surfactant concentration, c_e. The binding isotherm can be determined only below the critical micelle formation concentration (c_e < cmc) because above the cmc both the bound surfactant and the free micelles formed in the system is involved in the calculated B values. The isotherm can be characterized with two binding steps. The binding starts from zero surfactant concentration according to a Langmuir-like isotherm and accelerates from 0.3-0.4 mM equilibrium surfactant concentration showing a second binding step.

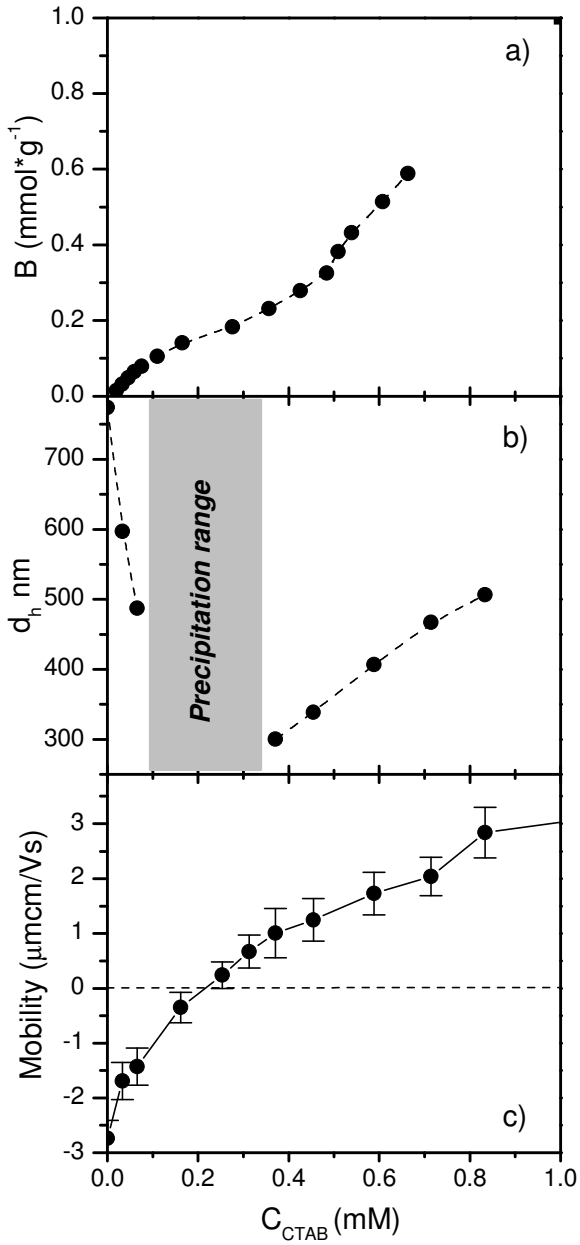

Fig. 30 a.) Binding isotherm of the CTAB on the nanogel latex (pH3,6). **b.)** Hydrodynamic size of the microgel particles (pH3,6) against the CTAB concentration. **c.)** The electrokinetic mobility of the microgel particles (pH3) against the CTAB concentration. All the three measurements where performed on a latex solution 0,02% w%

In the case of electrically neutral microgel/ionic surfactant interaction (such as e. g. pNIPAM homopolymer microgel interaction with sodium dodecyl sulfate[101] the interaction starts at a finite surfactant concentration (at the critical aggregation concentration, cac) indicating collective interaction (aggregate binding) of the surfactant with the polymer. In the case of the investigated microgel, an onset concentration of the surfactant binding (cac) cannot be identified, which implies that the surfactant binds in the charged microgel

particles in form of monomers during the first binding step. This type of interaction at low surfactant concentration can be interpreted by the contribution of the electrostatic interaction to the hydrophobic interactions.

In Fig. 31. the hydrodynamic size of the nanogel/surfactant complex is plotted against the surfactant concentration. The concentration axis practically corresponds to the equilibrium surfactant concentration because the experiments were performed at such a low latex concentration that the bound surfactant is negligible compared to the free monomer concentration. The d vs. c_{CTAB} function can be divided into three characteristic surfactant concentration ranges. First the size of the complex decreases and the system is stable. The deswelling of the microgel particles is caused by the surfactant binding, which results in a decreasing charge density within the microgel particles and as a consequence a decreasing osmotic pressure. In the second concentration range the coagulation of the latex can be observed (particle size can not be measured in this range due to the presence of macroscpic precipitates). The precipitation of the microgel is related to the fact that close to stoichiometric surfactant binding the particles loose their surface charge as it is indicated by the electrophoretic mobility measurements (Fig. 32), thus they loose their colloid stability giving rise to the aggregation and precipitation of the microgel / surfactant complexes. With further increasing surfactant concentration the microgel particles are recharged (Fig. 32), the particles re-swell (Fig.31) and the binding measurements indicate a second surfactant binding step with an onset concentration (cac) of ~0.3-0.4 mM (Fig.30). Furthermore, it should be noted that dynamic light scattering measurements indicate stable, highly monodisperse samples in this surfactant concentration range, which implies the lack of aggregation. These results can be interpreted with a second cooperative binding step taking place within the microgel particles, which charges up the gel network and gives rise to the swelling and stabilization of the microgel / surfactant complexes.

III.3.2. Steric stabilization

As it is indicated by the investigation of the pNIPAm-co-10%AAc / CTAB system, charged microgel particles loose their colloid stability when close to stoichiometric binding occurs. In order to stabilize these microgel complexes we decided to form a shell of hydrophilic, uncharged polymer chains around the microgel particles. This shell can provide a steric stabilization for the collapsed microgel particles, further more it can suppress immune reactions. We choose the poly(ethylene oxide) methyl ether methacrylate (PEO_{45}MEMA)

macromonomer for the shell formation, which consists of a PEO chain linked to a methacrylate group by an ester bond.

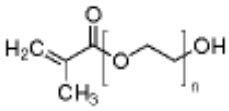

To form the PEO-shell around the microgel particles we used a step-like monomer feeding. First the microgel synthesis was initiated according to the normal synthetic procedure using the NIPAm, BA and AAc monomers. However, the PEO macromonomers were added to the reaction mixture only when most of the monomers have already reacted but the polymerization was still going on. To understand, which was appropriate moment to inject the macromonomer ($PEO_{45}MEMA$) to the reaction mixture the monomer conversion was investigated by HPLC .(Fig.33). It has been concluded that in agreement with the previous results the cross-linker monomer (BA) is the most reactive, however the rest of the monomers (NIPAm and AAc) have similar conversion rates. To test the formation of the PEO-shell we performed two syntheses. In the first one the PEO-macromonomer (10% of the total monomer concentration) was added to the reaction mixture after 12 minutes of polymerization (at ~80% conversion), and in the second case the macromonomers (5% of the total monomer concentration) was added to the reaction mixture after 20 minutes of polymerization (at ~90% conversion).

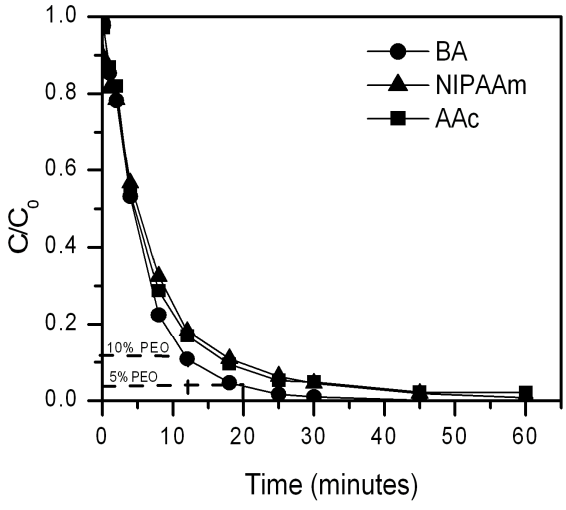

Fig. 33 Relative concentration of the unreacted monomers as a function of reaction time.

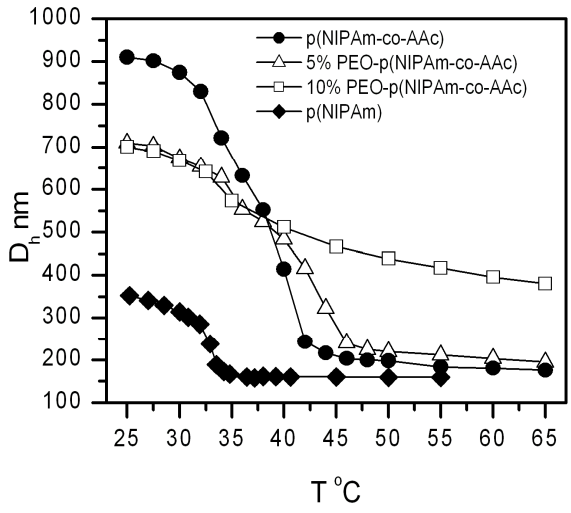

Fig.34 Hydrodynamic diameter of prepared pNIPAm based microgels.

In Fig. 34 the hydrodynamic size of the prepared pNIPAm microgel particles is shown as a function of temperature at a pH=4.5. The particles are in a swollen state at room temperature. As it is indicated by the figure the acrylic acid containing microgels have a much larger size at room temperature due to their charged nature. As the temperature increases and the VPTT is approached both the uncharged pNIPAm and the pNIPAm-co-10%AAc particles deswell and gel collapse occurs. As it is expected the charged pNIPAm-co-10%AAc microgels exhibit a higher VPTT due to the presence of the charged carboxylic groups.

The pNIPAm-co-10%AAc-shell-PEO microgels show a double VPT. The first step of deswelling coincides with the deswelling of the p(NIPAm-co-10%Aac) particles. However, full collapse does not occur but a second step of deswlling follows, which gives rise to fully collapsed microgel particles only in the case of 5% PEO_{45}MEMA content in the investigated temperature range. These observations are in agreement with the formation of a PEO containing outer shell on the microgel particles. The first step of deswelling corresponds to the collapse of the particle core that has an identical composition to that of the pNIPAm-co-10%AAc. The second step of deswelling is characteristic for the PEO containing outer shell. Since the PEO is a hydrophilic polymer its presence in the shell increases the VPTT and the increase is larger when more PEO is incorporated into the shell.

To check the alleged monodispersity of the prepared microgel particles we have centrifuged the latex solution at 40 ^{o}C for 60 minutes at 18000 rpm, then we left the samples stand at room temperature for 24 hours. Monodisperse soft particles could be packed in ordered closed packed structures giving rise to iridescent samples. As it is shown in fig. 35 each of

the prepared microgels showed iridescence indicating the monodispersity of the prepared core-shell particles.

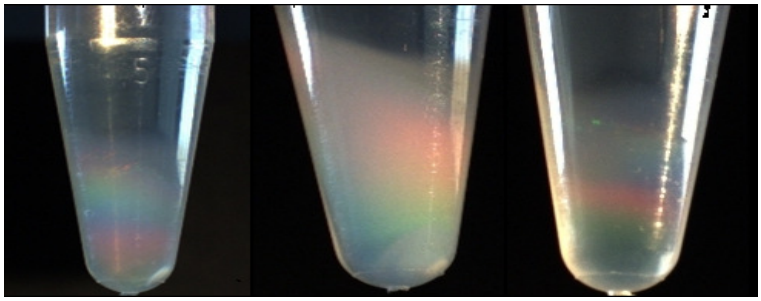

Fig.35 Irridescent colloid crystals of: 1) 5% PEO-p(NIPAm-co-AAc); 2)10% PEO-p(NIPAm-co-AAc); p(NIPAm-co-AAc)

To test the effect of the PEO-shell on the colloid stability of the microgel complexes the interaction of the 10% PEO containing microgel with DTAB was investigated. To enhance the attractive interaction of the microgel particles these investigations were performed above the collapse temperature of the uncharged gel network (40 °C). In Fig. 36 the size variation of p(NiPAm-co-AAc) microgel particles as a function of DTAB concentration is plotted. As its is indicated by the figure the particle collapse occurs at very low surfactant concentrations (~0.2 mM) but the colloid stability of the system is lost at only ~2mM DTAB concentration. With further increasing surfactant concentration phase separation occurs upto ~14 mM surfactant concentration, where the system will be stabile again.

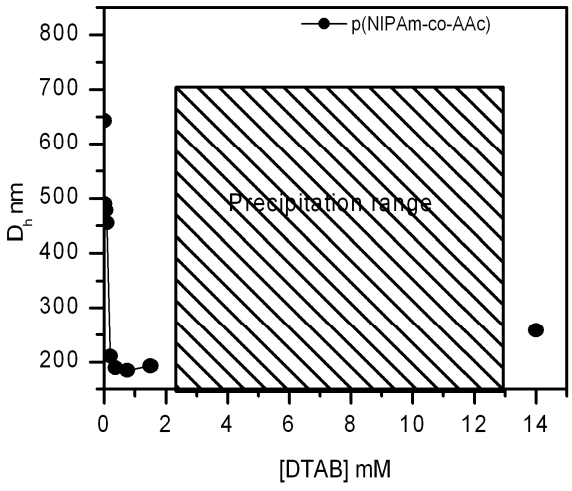

Fig.36 p(NiPAm-co-AAc) hydrodynamic diameter dependence on surfactant concentration

The phenomena can be better understood observing the electrophoretic mobility measurements reported in Fig.38. As the surfactant concentration increases the particle mobility continuously decreases but only at concentration values higher than 2mM the charge neutralization occurs, which leads to the loss of the colloid stability. Over ~14 mM the system recovers its stability due to further surfactant binding that leads to the recharging of the microgel particles.

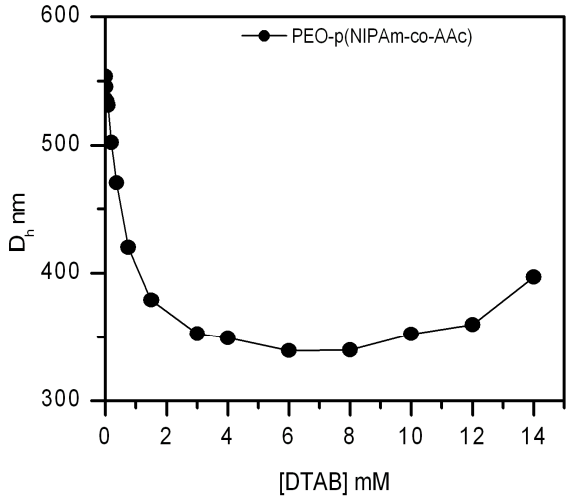

Fig. 37 p(NiPAm-co-AAc)-PEO hydrodynamic diameter dependence on surfactant concentration

Fig. 37 shows the size variation of p(NIPAm-co-10%AAc)-shell-10%PEO as a function of the surfactant concentration. The particles collapse as the surfactant concentration is less steep in this case and unlike the p(NIPAm-co-AAc) particles, the colloid stability is preserved for the whole surfactant concentration range. The system is stable even at those concentration values where the particles is fully neutralized by the bound surfactant (see Fig.38). When the surfactant concentration reaches ~15 mM the surfactant binding initiated re-swelling of the particles can also be observed.

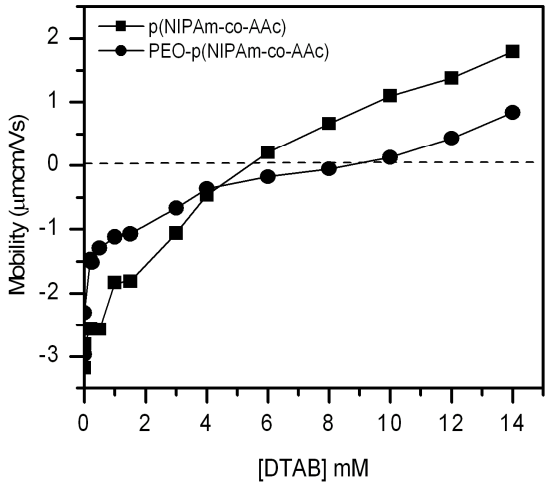

Fig.38 Electrophoretic mobility variation as a function of surfactant concentration of p(NIPAm-co-AAc) and PEO-p(NiPAm-co-AAc)

These results clearly demonstrate that the novel synthetic approach based on the step-like monomer feeding could be successfully employed to prepare microgel particles consisting of a p(NIPAm-co-10%AAc) core and a PEO shell. The PEO-shell formed on the microgel particles provides sufficient colloid stability even for the uncharged collapsed microgel particles.

SUMMARY

The major objective of my PhD work was to develop novel approaches for controlling the internal structure of individual microgel particles, as well as microgel multilayers.

One of the major contributions of my work has been that LbL-films can be successfully constructed from cationic cellulose nanofibrils and anionic poly-(N-isopropylacrylamide-*co*-acrylic acid) nanogel beads. It was found that the MFC fibers due to their rigid structure and relatively big size, 5-10 nm thickness and up to 1 μm length, cannot penetrate into the microgel particles thus cannot inhibit their volume phase transition. The lack of the interpenetration of the oppositely charged components gives rise to the formation of an open composite structure that is highly penetrable for other molecules. This was demonstrated by loading the multilayers with fluorescein isothio-cyanate and measuring the release kinetics at room temperature as well as by temperature cycling to induce the particle collapse. The nanogel films can load and release the dye at constant room temperature, which is in contrast to previously reported systems based on synthetic polyelectrolytes. The release was found relatively fast (took a few hours) and the released amount was directly proportional to the number of deposited double layers. It was also found that by collapsing the deposited microgel particles a close to quantitative release could be achieved in a single step.

Another important contribution of my work is the development of a novel synthetic method for the preparation of homogenously cross-linked microgel particles. The proposed method is based on keeping the NIPAm monomer and the BA cross-linker monomer concentrations constant within the reaction mixture, thus facilitating the constant rate of monomer incorporation for both components. The constant monomer concentrations are ensured by the continuous feeding of the monomers to the reactor. The optical properties and the swelling of the prepared homogenously cross-linked microgel particles significantly differ from the characteristics of the inhomogenously cross-linked microgels prepared with identical average crosslink density using the normal batch precipitation polymerization.

Finally a single-step synthetic procedure was developed for the preparation of sterically stabilized, monodisperse charged core / PEO-shell microgel particles. To demonstrate the formation and efficiency of the PEO-shell the colloid stability of oppositely charged p(NIPAm-co-10%AAc) / CTAB complexes and p(NIPAm-co-10%AAc-shell-PEO) / CTAB

complexes were investigated and compared. It has been shown that with increasing surfactant concentration first the complexes approach charge neutralization then become overcharged. However, in the charge neutral range the bare microgel / CTAB complexes lost their colloid stability and precipitated, while the particles with the PEO-shell preserved their collid stability in the entire surfactant concentration range.

LIST OF PUBLICATIONS

1. Attila Borsos, **Roberta Acciaro**, Róbert Mészáros, Tibor Gilányi „*Interaction of Cetyl Trimethylammonium Bromide With Poly-(N-Isopropylacrylamide-Co-Acrylic Acid) Copolymer Nanogel Particles"*, Progr. Colloid Polym. Sci., **2008**, *135*, 188–193.

2. **Roberta Acciaro**, Christian Aulin, Per M. Claesson, Lars Wågberg., Imre Varga "*Investigation of the formation, structure and release characteristics of self-assembled composite films of cellulose nanofibrils and temperature responsive microgels*" Soft Matter, **2011**, *7*, 1369 – 1377.

3. **Roberta Acciaro**, Tibor Gilanyi, Imre Varga "*Preparation of monodisperse p(N-isopropyl acrylamide) microgel particles with homogeneous segment density distribution*" Langmuir, **2011**, *Accepted.*

REFERENCES

[1] S. H. Gehrke, *Adv. Polym. Sci*. **1993**, *110*, 82

[2] A. S. Hoffman, *Adv. Drug Delivery Rev*. **2002**, *54*, 3

[3] K. Yeomans, *Chem. Rev.,* **2000**, *100*, 2

[4] D. Campoccia, P. Doherty, M. Radice, P. Brun, G. Abatangelo and D. F. Williams, Semisynthetic Resobable Materials from Hyarulonan Esterification, *Biomaterials,* **1998,** *19,* 2101

[5] G.D. Prestwich, D.M. Marecak, J.F. Marecak, K.P. Ver- [47] L.C. Dong, A.S. Hoffman, Q. Yan, Macromolecular penetracruysse, M.R. Ziebell, Controlled chemical modification of tion through hydrogels, J. Biomater. Sci. Polym. Ed. 5 hyaluronic acid, *J. Controlled Release,* **1998,** *53*, 93–103

[6] W. E. Hennink, C. F. van Nostrum, *Adv. Drug Delivery Rev*., **2002**, *54,* 13.

[7] Varga I, Gilanyi T, Meszaros R, Filipcsei G, Zrinyi M, *J.Phys.Chem.B*, **2001,** *105 (38),* 9071-9076

[8] Flory, P. J. *Principles of Polymer Chemistry*; Cornell University Press: Ithaca, NY, **1953**

[9] Schröder, U. P.; Oppermann, W. *Macromol. Chem., Macromol. Symp.* **1993**, *76*, 63.

[10] Tanaka, T. *Phys. Rev. Lett.,* **1978**, *40*, 820.

[11] P. *Bawa*, V. *Pillay*, Y. Choonara and L. Du Toit, *Biomed. Mater.,* **2009**, *4*, 022001

[12] Qiu Y and Park K., Environment-sensitive hydrogels for drug delivery *Adv. Drug. Deliv. Rev.,* **2001,** *53,* 321–39

[13] Chaterji S, Kwon K I and Park K., Smart polymeric gels: redefining the limits of biomedical devices *Prog. Polym. Sci.,* **2007,** ***32*** 1083–122

[14] M. Heskins, J.E. Guillet, *J. Macromol. Sci. Chem. A2,* **1968**, *8*, 1441-455.

[15] H.G. Schild, Poly(*N*-isopropylacrylamide): experiment, theory and application, Prog. Polym. Sci., **1992**, *17,* 163–249

[16] H. Feil, Y.H. Bae, S.W. Kim, Mutual influence of pH and temperature on the swelling of ionizable and thermosensitive hydrogels, *Macromolecules*, **1992**, *25*, 5528–5530

[17] Pagonis, Bokias, *Polymer***, 2004**, *45,* 2149-2153

[18] Zacharius S. L., ten Brinke, G., MacKnight, W. J. and Karasz, F. E., *Macromolecules* **1983**, *16*, 381

[19] Gupta P, Vermani K and Garg S., Hydrogels: from controlled release to pH-responsive drug delivery *Drug Discov. Today,* **2002***, 7***,** 569–79

[20] H. G. Schild, *Prog. Polym. Sci.,* **1992,** *17*, 163–249.

[21] Kratz K., Hellweg T., Eimer W., *Colloids and Surfaces***, 2000,** *170,* 137–149

[22] Tanaka T, Nishio I, Sun S T and Ueno-Nishio S., Collapse of gels in an electric field *Science,* **1982***, 218,* 467–9

[23] Gong J P, Nitta T and Osada Y., Electrokinetic modeling of the contractile phenomena of polyelectrolyte gels. One-dimensional capillary model *J. Phys. Chem.* **1994** *, 98* **,**9583–7

[24] I.C. Kwon, Y.H. Bae, T. Okano, S.W. Kim, Drug release from electric current sensitive polymers, J. Controlled Release *17* (**1991**) 149–156.

[25] A. Mamada, T. Tanaka, D. Kungwachakun, M. Irie, Photo induced phase transition of gels, *Macromolecules,* **1990**, *23,* 1517–1519

[26] A.A. Obaidat, K. Park, Characterization of glucose dependent gel–sol phase transition of the polymeric glucose– concanavalin A hydrogel system, *Pharm. Res.* **1996,** *13* 989–995.

27] Tanaka, T.; Fillmore, D. J. *J. Chem. Phys.* **1979**, *70*, 1214 - 1218

[28] Piyush Gupta, Kavita Vermani and Sanjay Garg, DDT Vol. 7, No. 10 May 2002

[29] Zhou G, Veron L, Elaissari A, Delair T, Pichot C., *Polym Int.,* **2004**, *53,* 603

[30] Urry, D. W., *Angew. Chem., Int. Ed. Engl*., **1993**, *32,* 819–841

[31] Richter A., Paschew G., Klatt S., Lienig J., Arndt K.F., Adler A.J.P., *Sensors* **2008***, 8*, 561

[32] Takei, Y. G. *et al*. *Macromolecules,* **1994,** *27*, 6163–6166

[33] C. Wu, S. Zhou, *Macromolecules* **1997**, *30,* 574

[34] Zhou S, Chu B., Synthesis and volume phase transition of poly(methacrylic-co-N-isopropylacrylamide) microgel particles in water. *J Phys Chem,* B **1998**;*102*,1364–71

[35] Das M, Sanson N, Fava D, Kumacheva E. Microgels loaded with gold nanorods: photothermally triggered volume transitions under physiological conditions. *Langmuir,* **2007**, *23(1),*196–201

[36] Hoare T, Pelton R. Highly pH and temperature responsive microgels functionalized with vinylacetic acid. *Macromol.* **2004,** *37,* 2544–50

[37] Höfl S, Zitzler L, Hellweg T, Herminghaus S, Mugele Frieder. Volume phase transition of “smart” microgels in bulk solution and adsorbed at an interface: a combined AFM, dynamic light, and small angle neutron scattering study. *Polymer,* **2007,** *48,* 245

[38] Karg M, Pastoriza-Santos I, Rodriguez-González B, von Klitzing R, Wellert S, Hellweg T. Temperature, pH, and ionic strength induced changes of the swelling behavior of PNIPAM-poly(allylacetic acid) copolymer microgels. *Langmuir*, **2008,** *24,* 6300

[39] W. McPhee, K.C. Tam, R. Pelton, *J. Colloid Interface Sci,***1993**, *156*, 24

[40] R. H. Pelton, P. Chibante, *Colloids Surf.* **1986**, *20,* 247

[41] J.W. Vanderhoff, H.L. Tarkowski,. J.B. Shaffer,. E.B. Bradford *and* R.M.. Wiley, *Adv.Chem.,* Ser.34, **1962**, 32.

[42] N. Dingenouts, S. Seelenmeyer, I. Deike, S. Rosenfeldt, M. Ballau, P. Lindner, T. Narayanan, *Phys. Chem. Chem. Phys*. **2001**, *3,* 1169

[43] X. C. Xiao, L. Y. Chu, W. M. Chen, S. Wang, R. Xie, *Langmuir* **2004,** *20*, 5247.

[44] L. Zha, Y. Zhang, W. Yang, S. Fu, *Adv. Mater*. **2002**, *14*, 1090

[45] C. D. Jones, L. A. Lyon, *Macromolecules* **2000**, *33*, 8301

[46] I. Berndt, W. Richtering, *Macromolecules* **2003**, *36,* 8780

[47] Wu X, Pelton RH, Hamielec A.E, Woods D.R., McPhee W. *Colloid PolymSci,* **1994,** *272*, 467

[48] B. R. Saunders, B. Vincent, *Adv. Colloid Interface Sci.* **1999**, *80*,1.

[49] H. M. Crowther, B. Vincent, *Colloid Polym. Sci.* **1998**, *276*, 46.

[50] Crowther, H. M., Saunders, B. R., Mears, S. J., Cosgrove, T., Vincent, B., King, S. M., Yu, G. E. *Colloids Surf, A Physicochem Eng Asp* **1999,** *152(3),* 327–33

[51]Kratz, K., Hellweg, T., Eimer, W., *Polymer* **2001,** *42(15),* 6631–9

[52] Kratz, K., Lapp, A., Eimer, W., Hellweg, T., *Colloids Surf, A Physicochem Eng Asp* **2002,** *197(1–3),* 55–67

[53] Fernandez-Barbero, A., Fernandez-Nieves, A., Grillo, I., Lopez-Cabarcos, E. *Phys Rev* **2002;** *E 66(5),* 051803

[54]Saunders, B. R. *Langmuir* **2004**, *20,* 3925

[55] Stieger, M., Richtering, W., Pedersen, J. S., Lindner, P. *J. Chem. Phys.* **2004,** *120(13),* 6197–6206

[56] B.R. Saunders, *Advances in Colloid and Interface Science*, **2009,** *147–148,* 251–262

[57] Hoare T, McLean D. Multi-component kinetic modeling for controlling local compositions in thermosensitive polymers. *Macromol Theory Simu.,l* **2006**, *15 (8)*, 619–32

[58] Gilanyi, T., Meszaros, R., Varga, I. *Colloid Polym Sci.* **2001,** *117,* 13

[59] Meszaros R., *Langmuir*, **2003**, *19 (3),* 609–615

[60] Ozin, G. A.; Yang, S. M. *Adv. Funct. Mater.* **2001**, *11*, 95-104

[61] Yang, S. M.; Ozin, G. A. *Chem. Commun.* **2000**, 2507-2508

62] Hanken, H. G.; Corn, R. M. *Anal. Chem.* **1995**, *67*, 3767-3774

[63] Gupta, P.; Vermani, K.; Garg, S. *Drug Discov. Today* **2002**, *7*, 569-579

[64] Qiu, Y.; Park, K. *Adv. Drug Deliv. Rev.* **2001**, *53*, 321-339

[65] Peppas, N. A. *Curr. Opin. Colloid Interface Sci.* **1997**, *2*, 531-537

[66] Malinsky, M. D.; Kelly, K. L.; Schatz, G. C.; Van Duyne, R. P. *J. Am. Chem. Soc.* **2001**, *123*, 1471-1482.

[67] Larsson, C.; Rodahl, M.; Hook, F. *Anal. Chem.* **2003**, *75*, 5080-5087

[68] Moller, G.; Harke, M.; Motschmann, H.; Prescher, D. *Langmuir* **1998**, *14*, 4955- 4957

[69] Roberts, C.; Chen, C. S.; Mrksich, M.; Martichonok, V.; Ingber, D. E.; Whitesides, G. M. *J. Am. Chem. Soc.* **1998**, *120*, 6548-6555

[70] G. Decher, *Science,* **1997**, *277*, 1232–1237

[71] V. Nerapusri, J. L. Keddie, B. Vincent and I. A. Bushnak, *Langmuir*, **2006**, *22*, 5036

[72] S. Schmidt, T. Hellweg and R. von Klitzing, *Langmuir*, **2008**, *24*,12595–12602

[73] M. J. Serpe, C. D. Jones and L. A. Lyon, *Langmuir*, **2003**, *19*, 8759–8764;

[74] C. M. Nolan, M. J. Serpe and L. A. Lyon, *Biomacromolecules*, **2004**, *5,* 1940–1946.

[75] M. J. Serpe, K. A. Yarmey, C. M. Nolan and L. A. Lyon, *Biomacromolecules*, **2005**, *6*, 408

[76] J. Wiedemair, M. J. Serpe, J. Kim, J.-F. Masson, L. A. Lyon, B. Mizaikoff and C. Kranz, *Langmuir,* **2007**, *23*, 130–137.

[77] C. D. Sorrell and L. A. Lyon, *J. Phys. Chem. B*, **2007**, *111*, 4060–4066

[78] J. E. Wong and W. Richtering, *Prog. Colloid Polym. Sci.,* **2006**, *133*, 45–51.

[79] P. Masse and S. Ravaine, *Colloids Surf.,* A, ***2005****, 270–271*, 148

[80] L. Wagberg, G. Decher, M. Norgren, T. Lindstrom, M. Ankerfors and K. Axnas, *Langmuir*, **2008**, *24*, 784

[81] C. Aulin, I. Varga, P. M. Claesson, L. Wagberg and T. Lindstrom, *Langmuir,* **2008**, 24, 2509

[82] C. Aulin, E. Johansson, L. Wagberg and T. Lindstrom, *Biomacromolecules*, **2010**, *11*, 872

[83] C. Aulin, S. Ahola, P. Josefsson, T. Nishino, Y. Hirose, M. Osterbergand L. Wagberg, *Langmuir,* **2009**, *25*, 7675–7685

[84] I. Sir_o and D. Plackett, Cellulose, 2010, 17, 459–494; A. Dufresne, *Can. J. Chem.,* **2008**, *86*, 484–494; A. N. Nakagaito and H. Yano, *Appl. Phys. A: Mater. Sci. Process.,*

2004, *80*, 155–159; M. Henriksson and L. A. Berglund, *J. Appl. Polym. Sci.,* **2007**, *106*, 2817–2824; A. J. Svagan, M. A. S. A. Samir and L. A. Berglund, *Biomacromolecules*, **2007**, *8*, 2556–2563; L. Berglund. Cellulosebased Nanocomposites, *CRC Press, US*, **2005**.

[85] A. F. Turbak, F.W. Snyder and K. R. Sandberg, *J. Appl. Polym. Sci.: Appl. Polym. Symp.,* **1983**, *37*, 815

[86] F. W. Herrick, R. L. Casebier, J. K. Hamilton and K. R. Sandberg, *J. Appl. Polym. Sci.: Appl. Polym. Symp.,* **1983**, *37*, 797

[87] Davidson CJ, Meares P, *J. Membrane* , **1988,** *36,* 511

[88] R. von Klitzing, *Phys. Chem. Chem. Phys.,* **2006**, *8,* 5012–5033.

[89] L. Wagberg, G. Decher, M. Norgren, T. Lindstrom, M. Ankerfors and K. Axnas, *Langmuir*, **2008**, *24*, 784–795.

[90] M. Paakko, M. Ankerfors, H. Kosonen, A. Nykanen, S. Ahola,M. Osterberg, J. Ruokolainen, J. Laine, P. T. Larsson, O. Ikkala and T. Lindstrom, *Biomacromolecules*, **2007**, *8*, 1934–1941

[91] S. Schmidt, H. Motschmann, T. Hellweg and R. von Klitzing, *Polymer*, **2008**, *49,* 749

[92] J. Wiedemair, M. J. Serpe, J. Kim, J.-F. Masson, L. A. Lyon, B. Mizaikoff and C. Kranz, *Langmuir*, **2007**, *23,* 130–137

[93] V. Nerapusri, J. L. Keddie, B. Vincent and I. A. Bushnak, *Langmuir,* **200**6, *22*, 5036–5041

[94] Hook, B. Kasemo, T. Nylander, C. Fant, K. Sott and H. Elwing, Anal. Chem., **2001**, *73*, 5796–5804

[95] H. Brewer, W. R. Glomm, M. C. Johnson, M. K. Knag and S. Franzen, Langmuir, **2005**, *21*, 9303–9307

[96] J. Serpe, K. A. Yarmey, C. M. Nolan and L. A. Lyon, *Biomacromolecules*, **2005**, *6*, 408–413.

[97] Hoare, T., Pelton, R. *Curr. Opin. Colloid Interface Sci.* **2008,** *13,* 413–428

[98] Saunders, B. R.; Daly, N. L., E.; Hu, S. T., X.; Stepto, R. *Adv. Colloid Interface Sci.* **2009,** *147–148,* 251

[99] Inomata, H.; Wada, N.; Yagi, Y.; Goto, S.; Saito, S. *Polymer* **1995**, *36*, 875; Senff, H.; Richtering, W. *Colloid Polym. Sci.* **2000**, *278*, 821

[100] Justin D. Debord and L. Andrew Lyon *J. Phys. Chem. B,* **2000,** *104,* 6327

[101] Gilányi T, Varga I, Mészáros R, Filipcsei G, Zrinyi M, *Langmuir* **2001**, *17*, 4764